Unearthing Foundations of a Cosmic Cathedral: Searching the Stars for M33's Halo

Robert Cockcroft

Department of Physics and Astronomy, McMaster University, Hamilton, Ontario, L8S 4M1, Canada

cockcroft@physics.mcmaster.ca

Alan W. McConnachie

NRC Herzberg Institute of Astrophysics, 5071 West Saanich Road, Victoria, British Columbia, V9E 2E7, Canada

alan.mcconnachie@nrc-cnrc.gc.ca

William E. Harris

Department of Physics and Astronomy, McMaster University, Hamilton, Ontario, L8S 4M1, Canada

harris@physics.mcmaster.ca

Rodrigo Ibata

Observatoire Astronomique, Universit de Strasbourg, CNRS, 11, rue de l'Universit, F-67000 Strasbourg, France

ibata@astro.u-strasbg.fr

Mike J. Irwin

Institute of Astronomy, University of Cambridge, Madingley Road, Cambridge CB3 0HA, UK

mike@ast.cam.ac.uk

Annette M. N. Ferguson

Institute for Astronomy, University of Edinburgh, Blackford Hill, Edinburgh, EH9 3HJ, UK

ferguson@roe.ac.uk

Mark A. Fardal

Department of Astronomy, University of Massachusetts, 710 North Pleasant Street, Amherst, MA, USA

fardal@astro.umass.edu

Arif Babul

Department of Physics and Astronomy, University of Victoria, Victoria, BC, V8P 1A1, Canada

babul@uvic.ca

Scott C. Chapman

Institute of Astronomy, University of Cambridge, Madingley Road, Cambridge CB3 0HA, UK

schapman@ast.cam.ac.uk

Geraint F. Lewis

Institute of Astronomy, School of Physics, A28, University of Sydney, NSW 2006, Australia

gfl@physics.usyd.edu.au

Nicolas F. Martin

Max-Planck-Institut fr Astronomie, Knigstuhl 17, D-69117 Heidelberg, Germany

martin@mpia.de

and

Thomas H. Puzia

Department of Astronomy and Astrophysics, Pontificia Universidad Catlica de Chile, Av. Vicuna Mackenna 4860, 7820436 Macul, Santiago, Chile

tpuzia@gmail.com

ABSTRACT

We use data from the Pan-Andromeda Archaeological Survey (PAndAS) to search for evidence of an extended halo component belonging to M33 (the Triangulum Galaxy). We identify a population of red giant branch (RGB) stars at large radii from M33's disk whose connection to the recently discovered extended "disk substructure" is ambiguous, and which may represent a "bona-fide" halo component. After first correcting for contamination from the Milky Way foreground population and misidentified background galaxies, we average the radial density of RGB candidate stars over circular annuli centered on the galaxy and away from the disk substructure. We find evidence of a low-luminosity, centrally concentrated component that is everywhere in our data fainter than $\mu_V \sim 33$ mag arcsec^{-2}. The scale length of this feature is not well constrained by our data, but it appears to be of order $r_{exp} \sim 20$ kpc; there is weak evidence to suggest it is not azimuthally symmetric. Inspection of the overall CMD for this region that specifically clips out the disk substructure reveals that this residual RGB population is consistent with an old population with a photometric metallicity of around [Fe/H] $\sim$ -2 dex, but some residual contamination from the disk substructure appears to remain. We discuss the likelihood that our findings represent a bona-fide halo in M33, rather than extended emission from the disk substructure. We interpret our findings in terms of an upper limit to M33's halo that is a few percent of its total luminosity, although its actual luminosity is likely much less.

Subject headings: galaxies: evolution – galaxies: halos – galaxies: individual (M33) – galaxies: spiral – Local Group

1. Introduction and Background

Λ Cold Dark Matter (ΛCDM) cosmology predicts that larger galaxies are built through the hierarchical merging of smaller galaxies. Infalling components are disrupted partially or entirely, and part of that material forms the stellar halo of the larger galaxy. Stellar halos therefore contain the remnants of past interactions between galaxies, and their properties can indicate the approximate time, size and frequency of past mergers (e.g., Purcell et al. 2007).

We can directly observe only a few relatively nearby halos in any great detail due to their faint nature, and only a small number of halos are directly observed through their resolved stars outside of the Local Group. Due to their faintness, it is problematic to determine whether or not the halos are smooth and/or symmetric. There is likely a continuum of scenarios that we observe between newly-accreted objects (creating streams, shells, etc.; e.g., Martínez-Delgado et al. 2010) and smooth halos, and our interpretation will depend on the time since the accretion and the spatial resolution and depth of the observations. The long dynamical timescales for structures outside of the disk implies that they are long-lived (Johnston et al. 1996).

Outside of the Local Group, halo detections are extremely challenging as it becomes more difficult with increasing distance to distinguish the halo from other stellar components (e.g., Dalcanton & Bernstein 2002; de Jong et al. 2008) and even more so in the absence of kinematical data (Barker et al. 2009, 2012). Scattered light and non-stellar pollution of counts also interfere with halo detections (e.g., de Jong 2008). (The surface brightness detection limits generally needed are ≥ 7 magnitudes fainter than the sky where the "darkest" skies (20th percentile), at Mauna Kea, are fainter than $\mu_V \gtrsim 21.3$.)[1]

---

[1]http://www.gemini.edu/sciops/telescopes-and-sites/observing-condition-constraints

Searches for halos around distant galaxies began with deep observations around single galaxies using surface brightness photometry and, as recent studies continue to do, focussed on late-type edge-on galaxies (e.g., Sackett et al. 1994; Shang et al. 1998; Zibetti & Ferguson 2004; Tikhonov & Galazutdinova 2005; Buehler et al. 2007; de Jong et al. 2007; Seth et al. 2007; Rejkuba et al. 2009; Mouhcine et al. 2007, 2010; Radburn-Smith et al. 2011). Each stellar component is revealed more easily in the cross-section rather than the face-on view. An alternative technique stacks many re-scaled images of galaxies together before looking for a halo signal (Zibetti et al. 2004; de Jong 2008; Bergvall et al. 2010; Zackrisson et al. 2011; Zackrisson & Micheva 2011), again highlighting the difficulty of detecting halos because of their extreme faintness.

Halos have also been observed around other types of galaxies, not just late-type edge-on galaxies: for example, the Virgo Cluster's central elliptical galaxy, M87 (Weil et al. 1997), nearby starburst galaxies (Bailin et al. 2011; Ryś et al. 2011; Rich et al. 2012), the Leo elliptical NGC 3379 (Harris et al. 2007), and the giant elliptical NGC 5128 (Centaurus A; see Malin et al. 1983; Peng et al. 2002; Rejkuba et al. 2011).

§ 2 provides a literature review of stellar halos in the Local Group. Details of the PAndAS observations around M33 are given in § 3. We are ultimately concerned with identifying the RGB stars in the M33 halo (if it exists). However, we must exclude the regions associated with the extended optical substructure surrounding the disk identified in McConnachie et al. (2009, 2010), and we must also correctly account for and subtract off the contribution from the foreground Milky Way disk and halo components, and the background galaxies misidentified as stars. § 4 describes these corrections and exclusions as part of the analysis. We discuss our results in § 5, before summarizing in § 6.

2. Halos of the Local Group Galaxies

2.1. The Milky Way Galaxy

The Local Group provides the closest opportunity to study a stellar halo but even the Milky Way (MW) is problematic to observe because of the restrictions and biases associated with viewing our Galaxy from within - although it has obviously been studied in depth (e.g., see the annual review by Helmi 2008, and references therein). Current seemingly contradictory evidence means it is unclear whether the MW stellar halo is oblate, prolate or triaxial (Newberg & Yanny 2006, Deason et al. 2011), although models of the dark matter (DM) halo seem to favour triaxiality (Law et al. 2009, Law & Majewski 2010). Numerous detections of substructure beyond the stellar bulge and disk are another reason that this ambiguity remains - substructure such as the Sagittarius dwarf galaxy (Ibata et al. 1994) and associated tidal streams (Ibata et al. 2001b, 2002; Majewski et al. 2003), the Monoceros ring (Ibata et al. 2003; Yanny et al. 2003; Crane et al. 2003), overdensities in Canis Major (Martin et al. 2004a,b) and Virgo (Vivas et al. 2001; Newberg et al. 2002; Xu et al. 2006; Jurić et al. 2008), clouds in the Triangulum-Andromeda region (Rocha-Pinto et al. 2004; Martin et al. 2007) and the Hercules-Aquila region (Belokurov et al. 2007a), and finally the Orphan (Grillmair 2006; Belokurov et al. 2006, 2007b) and Cetus Polar (Newberg et al. 2009) streams.

There is growing evidence to suggest that the MW halo has a dual halo, with the different components a result of their different formation processes (e.g., Chiba & Beers 2000; Carollo et al. 2007; Miceli et al. 2008; de Jong et al. 2010; Beers et al. 2012), such as satellite accretion and in-situ formation (e.g., Bell et al. 2008; Schlaufman et al. 2009, 2012; Zolotov et al. 2009; Oser et al. 2010; McCarthy et al. 2012).

The total (dark plus luminous) mass of the Galaxy within 300 kpc is estimated to be

in the range $0.7 \leq M_{MW} \leq 3.4$ x 10^{12} M$_\odot$ (Baiesi Pillastrini 2009; Watkins et al. 2010). The MW stellar halo luminosity, including all substructure, is estimated to be of order $L_{MW,halo,V} \sim 10^9 L_\odot$ (Carney et al. 1990; Bullock & Johnston 2005, and references therein), compared to the MW host luminosity, $L_{MW,host,V} = 2.1^{+1.0}_{-0.6}$ x $10^{10} L_\odot$ (Sackett 1997).

2.2.   The Andromeda Galaxy

Observations of the Andromeda and Triangulum Galaxies (M31 and M33, respectively) are free from the problems inherent with viewing the MW from within, but are still close enough to resolve individual stars (Mould & Kristian 1986; Crotts 1986) - and many ground-based studies are now also resolving individual stars beyond the Local Group (e.g., Barker et al. 2009, 2012; Bailin et al. 2011; Tanaka et al. 2011). However, progress on the study of M31's full extended stellar halo has only come relatively recently - and the degree to which it is similar to the MW's halo is still uncertain (Kalirai et al. 2006; Ibata et al. 2007; Koch et al. 2008). M31's total (dark plus luminous) mass is estimated to be in the range 9.0 x $10^{11} M_\odot < M_{M31} \lesssim 2$ x $10^{12} M_\odot$ (Evans & Wilkinson 2000; Chapman et al. 2006; Watkins et al. 2010). The lower limit is determined from the kinematics of RGB stars out to 60 kpc with 99% confidence (Chapman et al. 2006). An alternative dynamical mass that uses kinematics of M31's giant stream rather than those of the satellite galaxies, globular clusters, planetary nebulae or RGB stars, gives $M_{M31,R<125kpc} = 7.5^{+2.5}_{-1.3}$ x $10^{11} M_\odot$ (Ibata et al. 2004). M31 has a total host luminosity of $L_{M31,host,V} \sim 2.6$ x $10^{10} L_\odot$ (van den Bergh 1999), which is approximately 25% brighter than the MW. Many photometric substructures have been revealed around M31 (Ibata et al. 2001a; Ferguson et al. 2002; Irwin et al. 2005; Ibata et al. 2005, 2007; McConnachie et al. 2009). Irwin et al. (2005) fit minor-axis profiles of a de Vaucouleurs law out to a projected radius of $\sim$20 kpc, and beyond this a power law (index $\sim$ -2.3) or exponential (scale length

$\sim$ 14 kpc). Ibata et al. (2007) also find a smooth underlying component to which they fit a Hernquist profile (scale length $\sim$ 55 kpc), and a power law (index $\sim$ -1.91 $\pm$ 0.11), similar to the MW halo. If symmetric, Ibata et al. estimate that the total luminosity of the smooth halo is $L_{M31,halo,V} \sim 10^9 L_\odot$, again similar to the MW halo. More recently, Courteau et al. (2011) combine ground- and space-based data from several sources and decompose the resulting composite luminosity profile to find a halo component described by a power law (index $\sim$ -2.5 $\pm$ 0.2). M31's halo has further similarities to that of the MW's in terms of metallicity and velocity dispersion (Chapman et al. 2006). Using a Keck/DEIMOS sample of $\sim$800 stars, Chapman et al. find a non-rotating metal-poor ([Fe/H] $\sim$ -1.4) smooth halo between 10 - 70 kpc with no metallicity gradient underlying the metal-rich ([Fe/H] $\sim$ -0.9) rotating extended component. Along with a comparable dark matter halo mass, the similar metallicities and dispersions are suggestive that the early formation periods of both were also similar.

2.3. The Magellanic Clouds

The Large Magellanic Cloud (LMC) is the fourth most massive Local Group member. It has a total mass of $M_{LMC} \approx 10^{10} M_\odot$ (van der Marel et al. 2002; Bekki & Stanimirović 2009). The total host luminosity is $L_{LMC,host,V} = 3.0$ x $10^9 L_\odot$ (Bekki & Stanimirović 2009). It may also have a stellar halo. A study of RR Lyrae stars, generally associated with old and metal-poor stellar populations, finds that these stars have a large velocity dispersion of 53 $\pm$ 10 km s^{-1} (Minniti et al. 2003; Alves 2004). A photometric and spectroscopic survey has also revealed individual RGB stars enveloping the LMC out to large distances and consistent with a de Vaucouleurs profile, suggestive of a classical halo (Majewski et al. 2009). If the LMC does have a stellar halo it seems somewhat surprising given that another tracer of old and metal-poor populations - globular clusters - show no evidence for a halo as

they lie within a disk region around the LMC (Freeman et al. 1983; Schommer et al. 1992). This inconsistency could be explained if the GCs are accreted in earlier, more gas-rich merger events compared to those that populate the halo with individual stars (Bekki 2007).

The stellar outskirts of the Small Magellanic Cloud (SMC) have recently been studied through the MAgellanic Periphery Survey (MAPS; Nidever et al. 2011) to reveal a population of nearly azimuthally-symmetric RGB stars out to a radius of ∼11 kpc. The profile of these stars are well fitted with an exponential profile (scale length ∼1 kpc) out to ∼8 kpc, with a shallower profile beyond (scale length ∼7 kpc) - the latter of which the authors suggest could be a stellar halo or a population of extratidal stars.

2.4. The Triangulum Galaxy

M33, the Triangulum Galaxy, is the third most massive galaxy in the Local Group, with a mass close to one tenth that of M31 (Corbelli & Salucci 2000 measure M33's rotation curve out to 16 kpc, and find an implied dark halo mass of $M_{M33} \gtrsim 5$ x $10^{10} M_\odot$). M33 has a total host luminosity of $L_{M33,host,V} \sim 10^9 L_\odot$ (de Vaucouleurs et al. 1991) and is more face-on ($i = 56° \pm 1°$, Zaritsky et al. 1989) than M31 ($i = 77°$; e.g., Rubin et al. 1973; Athanassoula & Beaton 2006). It is classified as a SA(s)cd II-III galaxy (de Vaucouleurs et al. 1991), has little or no bulge component, a UV- and X-ray bright nuclear cluster (e.g., Long et al. 1981, Dubus et al. 1999 and Foschini et al. 2004), and perhaps a bar (Javadi et al. 2011), so most of the central light is distributed over an exponential disk component (e.g., de Vaucouleurs 1959; Bothun 1992; Minniti et al. 1993; McLean & Liu 1996; Corbelli et al. 2008; Kormendy et al. 2010; Javadi et al. 2011). The distance estimates to M33 cover a wide range from 730 ± 168 kpc (Brunthaler et al. 2005) to 964 ± 54 kpc (Bonanos et al. 2006). This disagreement appears to arise because of the combination of the different techniques used, and also perhaps due to inhomogeneous

interstellar extinction in M33. Consistent with McConnachie et al. (2010), we adopt a distance modulus for M33 of $(m − M_0) = 24.54 ± 0.06$ (809±24 kpc; McConnachie et al. 2004) throughout this paper. This distance is based on the TRGB method, and is consistent with our new findings (820^{+20}_{-19} kpc; Conn et al. 2012). At 809 kpc, $1°$ corresponds to 14.1 kpc.

Is there an M33 halo akin to those found in the MW, M31 and possibly the LMC? Previous claims of a detection for M33's halo have come from various sources, in studies that resolve individual stars (RGB or RR Lyrae stars), or globular clusters, which we briefly review here.

Mould & Kristian (1986) used the Hale Telescope/PFUEI to observe two fields both 7 kpc from the centre of each M31 and M33, along their southeast minor axes. By comparing the observed giant branches to those for M92 ($< [M/H] >= −0.6$) and 47 Tuc ($< [M/H] >= −2.2$), they inferred the presence of inner halos. However, Tiede et al. (2004) observed a field with WIYN/S2KB that included the region studied by Mould & Kristian and found that the peak of the MDF showed a radial variation with a gradient consistent with that of the inner disk region and *not* of an inner halo. Chandar et al. (2002) obtained WIYN/HYDRA spectra for 107 of M33's star clusters. These clusters, from a sample with known integrated HST/WFPC2 colors, were selected to cover the entire age range of M33's clusters (6 Myr to >13 Gyr; Chandar et al. 2001). Chandar et al. observed a large velocity dispersion that, with Monte Carlo simulations, suggested that old (> 1 Gyr) clusters could be split into two components which they associate with a disk population and the other with a halo. Similarly, Sarajedini et al. (2006) observed 64 RR Lyrae variable stars (type RRab) using HST/ACS to have a double peak in periods, again suggesting two subpopulations: a disk and a halo component. RR Lyrae stars are only observed in populations older than 10 Gyr, and therefore stars in these populations should be at least as old as the RR Lyraes.

Further hints of M33's halo also come from the following sources. Barker et al. (2007a,b) inspected three HST/ACS southeastern fields ∼20'-30' (∼4.7-7.1 kpc, assuming a distance to M33 of 809 kpc; McConnachie et al. 2004) from M33's nucleus. Mixed stellar populations were revealed in the CMDs, with an age range from < 100 Myr to a few Gyr. The authors compared synthetic populations with the observed CMDs, and found that the mean age increased with radius from ∼ 6 to 8 Gyr, and the mean metallicity decreased from ∼-0.7 to -0.9 dex. They concluded that while the fields are dominated by a disk population, a halo component may also be present. Cioni et al. (2008) used UKIRT/WFCAM near-infrared observations of a 1.8 degree^2 region centred on M33 to look at the ratio of C- to M-type AGB stars. They also found metallicity and age gradients such that the outer regions were more metal poor and a few Gyr older than the central regions, in agreement with Barker et al. (2007a,b). Ferguson (2007) reviews results for M31 and M33, and notes that while a halo-like component with a power-law structure was proving elusive, the RGB narrows and becomes more metal poor beyond ∼10 kpc. Teig (2008) used RGB and AGB star counts along M33's minor axis, and also observed a break in the surface brightness profile at 11 kpc. The profile at this region appeared to change from an exponential to a power-law. Barker et al. (2011) use HST/ACS to observe two fields 9.1 kpc and 11.6 kpc along M33's north major axis. They find that the outer field is old (7 ± 2 Gyr), moderately metal poor (mean $[M/H]$ ∼ -0.8 ± 0.3), and contained ∼30 times less stellar mass than the inner field. One of the interpretations that Barker et al. discuss is that the outer field is a transition zone from the outer disk to another structural component. Grossi et al. (2011) use Subaru/Suprime-Cam data with seven fields $10 \lesssim r < 30$ kpc from the centre of M33 in the NW and SE. An exponential scale length of ∼7 kpc is found for both regions, and these authors favour that this component is an extended disk rather than a halo.

The previous section highlights that unambiguous detections of the various galactic

components - even for one of our closest neighbouring galaxies - are still extremely difficult. While studies of star clusters and RR Lyrae stars show evidence for an old halo, studies of individual stars in other subpopulations have only been marginally conclusive. Part of the problem was the limited coverage and/or depth.

McConnachie et al. (2006) undertook a spectroscopic survey of RGB stars using Keck/DEIMOS. Radial velocity distributions of these stars were best-fit by three Gaussian components, which McConnachie et al. interpreted as contributions from a halo, a disk, and a component offset from the disk (which they suggested could have been a stellar stream or another stellar halo component). Ibata et al. (2007) extended the observations of Ferguson et al. (2007) with CFHT/MegaCam along the southeastern corner of M31's halo out to M33's centre. Ibata et al. clearly saw the classical disk of M33, and in addition revealed an extended component. They fit a profile to the data between 1 and 4 degrees (the edge of the disk, and the point just before where the profile starts rising again, respectively) and found the exponential scale length to be 18 ± 1 kpc, or 55 ± 2 kpc using a projected Hernquist model. These scale lengths were surprisingly as big as they found for M31, although Ibata et al. cautioned that without a full panoramic view it was not possible to determine whether or not this feature was a "bona fide" halo.

Direct and unambiguous evidence for a stellar halo around M33 remains elusive but is the aim of this paper. Any such component must be quite faint. We extend the work begun by McConnachie et al. (2009, 2010) as part of the Pan-Andromeda Archaeological Survey (PAndAS), which itself built on previous surveys with the INT/WFC (Ferguson et al. 2007) and CFHT/MegaCam (Ibata et al. 2007). Optical observations prior to PAndAS suggested M33's disk had an undisturbed appearance - a view that persisted until relatively recently (e.g., Sarajedini 2007; Ferguson et al. 2007). This implied that the disk had not been tidally disrupted by either the MW or M31, and was seemingly discrepant when compared

to the radio detection of a warped gaseous disk component (e.g., Rogstad et al. 1976; Putman et al. 2009). We note, however, that the primary problem with the Ferguson et al. data set was depth and that the observations could only rule out the presence of substructure or a halo with surface brightnesses brighter than $\mu_V \sim 31$ mag arcsec^{-2}.

PAndAS observations covering the area around M33 with unprecedented combination of depth and coverage have revealed a vast low surface brightness stellar substructure. The S-shaped optical warp of this substructure is generally aligned with the HI warp, and therefore resolves the previous discrepancy. It now seems most likely that this warp was the feature that was previously partially detected by McConnachie et al. (2006) (thereby casting doubt on the previous interpretations from this kinematic study) and Ibata et al. (2007). Although the nature of the substructure is still being investigated, the favoured interpretation for its origin is that it is a disruption of the disk that was caused by a tidal interaction with M31 as M33 orbits M31 (McConnachie et al. 2009, 2010; Dubinski et al. in prep.). Preliminary models can reproduce the shape of the extended disk substructure, and also satisfy M33's proper motion constraints (Brunthaler et al. 2005). Spectroscopic observations may provide further clues (see upcoming paper by Trethewey et al. 2012).

The depth of the PAndAS data allows us to test whether or not a genuine halo component is observable in addition to the disk-like warp. Given that the warped extended disk substructure is extremely faint and had eluded detection for so long, it would be reasonable to expect any underlying component of a halo to also be extremely faint. Indeed, a faint extended stellar component is hinted at beyond the extended disk substructure, and one possibility put forward is that this is a halo component (McConnachie et al. 2010).

Since M33 is relatively low mass, would we expect it to have a detectable halo? Purcell et al. (2007) predict that a galaxy with total mass $M \sim 10^{11} M_\odot$ will, *on average*, have a halo that contributes $\leq 1\%$ of the total luminosity from the galaxy. Therefore, the

expected total halo luminosity of M33 could be as low as $L_{M33,halo} \leq 10^7 L_\odot$. Their halo estimates make no distinction between the smooth component and the substructure. Here, we *define* the "halo" as the component or stellar population in the outer regions of M33 that is not clearly associated with the disk or the extended disk substructure identified by McConnachie et al. (2010). Note that we do not distinguish between smooth or lumpy halos, similarly to Purcell et al. (2007).

3. Observations, Data Reduction and Calibration

We use data from the Pan-Andromeda Archaeological Survey (PAndAS; McConnachie et al. 2009) to observe 48 degree^2 around M33 with CFHT/MegaCam out to a projected radius of 50 kpc (cf. $r_{M33,virial} = 152$ kpc, Martin et al. 2009). The data has limiting magnitudes for point-source detections of $g' \approx 25.5, i' \approx 24.5$ (AB magnitudes on the SDSS scale) at S/N = 10 in subarcsecond seeing. MegaCam is composed of 36 individual CCDs, has a 0.96 x 0.94 degree field of view and a resolution of 0.187" pixel^{-1}.

Figure 1 shows each location of the MegaCam $\sim$square-degree images around M33 in a tangent-plane projection. To be explicit, for our analysis we only consider the data for MegaCam images within the annulus with radius 3.75 degrees centred on M33 as shown in Figure 1. The MegaCam subexposures are dithered in order to cover the small gaps, but not the large gaps[2]. In the large gaps there may be fewer detections due to shallower depths. However, the area of the chip gaps is very small compared to the overall MegaCam field and can be neglected for the purposes of this analysis.

The prefixes of the image labels in Figure 1 represent the timeline of the observations: The central field, m33c, was observed primarily in the observing semester 2004B and

---

[2]See http://www.cfht.hawaii.edu/Instruments/Imaging/Megacam/specsinformation.html

retrieved from the CFHT archive, with some data from 2003B. All other fields with prefix m were observed in 2008B. Fields with prefix nb were observed in 2009B. Due to a failure of CCD 4 in the 2003B observing semester, the data from Ibata et al. (2007) which extended the southeastern section of M31's halo in a line to the centre of M33 was replaced with data from 2010B (prefix tb). The ellipse in Figure 1 marks the $\mu_B \approx 25$ mag arcsec^{-2} (Nilson 1973) contour of M33's disk, and the solid-line cross represents the major and minor axes of M33, with the major axis inclined 23 degrees to North (Nilson 1973). The dashed concentric circles represent radii at $r = 1, 2, 3$ and 3.75 degrees (14.1, 28.2, 42.4 and 53.0 kpc, respectively) from the centre of M33. The data within the annuli that they delineate will be used in the analysis that follows. M33 is approximately 31 degrees below the central axis of the Milky Way disk, M33$_{(l,b)}$ = (133.61, -31.33) degrees, compared with M31 which is about 21 degrees below, M31$_{(l,b)}$ = (121.18, -21.57) degrees. The three dashed lines in Figure 1 are lines of equal Galactic latitude (b = -35.3, -31.3 and -27.3 degrees).

Pre-processing and reduction were undertaken with Elixir[3] by the CFHT team, and by the Cambridge Astronomical Survey Unit (CASU) through a pipeline adapted for MegaCam images (Irwin & Lewis 2001), respectively. The reader is referred to McConnachie et al. (2009, 2010) and Cockcroft et al. (2011) for more details.

4.   Analysis

Taking advantage of the wide coverage of the PAndAS data, we deliberately seek direct evidence for M33's stellar halo in this data, and expect it to be extremely faint, centrally-concentrated, and detectable via RGB stars. However, this low-luminosity component will be mixed with stars from the M33 disk, M33 extended disk substructure

---

[3]http://www.cfht.hawaii.edu/Instruments/Imaging/MegaPrime/dataprocessing.html

surrounding the disk, and the MW foreground (both its thick disk and halo), in addition to background galaxies misidentified as stars. Our technique involves statistically removing the MW foreground stars and background galaxies, excluding the regions identified as belonging to M33's extended disk substructure, and seeing what signal remains.

Figure 2 shows the colour-magnitude (Hess) diagrams for the data in the annuli in Figure 1. We note that Figure 2 contains more than 1.4 million objects that were identified as robust stellar candidates in both g_0 and i_0 through the CASU pipeline's object morphological classification. Magnitudes are de-reddened source by source using values of $E(B-V)$ in the range $0.034 \leq E(B-V) \leq 0.130$, with $g_0 = g$ - 3.793 $E(B-V)$ and $i_0 = i$ - 2.086 $E(B-V)$ (Schlegel et al. 1998). The data is binned in 0.025 x 0.025 mag bins and is shown with a logarithmic scale for the number counts of stars. As mentioned previously, we want to identify M33 RGB stars but first we need to estimate the level of contamination. To examine the MW foreground contamination, we look at the two sources of contribution from MW stars easily identifiable in the CMDs. The MW halo turn-off stars are seen as a thin band on the left of the CMDs, and we use a region defined as 0.1 $< (g-i)_0 < 0.6$, $19 < i_0 < 22$ to measure their relative numbers in each zone. The red MW disk dwarfs are seen as a broader band on the right, and we identify them in the region $1.5 < (g-i)_0 < 3$, $17 < i_0 < 20$. Both of the regions for the MW disk and halo stars are consistent with McConnachie et al. (2010). Finally, M33 RGB stars are selected by the colour-magnitude locus where we would expect to find RGB stars. This locus is defined using isochrones from the Dartmouth Stellar Evolution Database (Dotter et al. 2007, 2008) which are transformed to the CFHT photometric system (McConnachie et al. 2010). These isochrones are between the 12 Gyr $[\alpha/\text{Fe}] = 0.0$ isochrones, shifted to the M33 distance modulus, with metallicities of -2.5 dex $< [Fe/H] < $ -1 dex. This is a necessarily broad cut to allow for the possible range of metallicities that may be present in M33's halo, which we expect to be predominantly metal poor. Note that metal-rich stars may also be present,

but will likely contribute a small amount to the overall halo component, while increasing dramatically the contamination from foreground stars that occupy a similar locus in the CMD. We could expect some α-enhancement in the M33 halo, as we see in the MW halo (e.g., Venn et al. 2004), but since there is no evidence to suggest this we adopt $[\alpha/\text{Fe}] = 0.0$ for simplicity. We also note that the isochrones are being used to help define a locus in the CMD, and an absolute interpretation of the implied metallicities is not intended (for example, there will also be age degeneracies). A magnitude limit of $21.0 < i_0 < 24.0$ is also imposed on the RGB candidate stars, with the lower limit ensuring a high level of completeness while excluding the majority of bright background galaxies mis-identified as stars (which becomes a major source of contamination at faint magnitudes; $i_0 \approx 25$, $0 \lesssim i_0 \lesssim 1$). We test the effect of raising the faint limit to $i_0 < 23.5$ in Section 4.3.

The four panels in Figure 2 correspond to annuli with the radii between $r = 0\text{-}1$, 1-2, 2-3 and 3-3.75 degrees. We use the latter annulus to estimate the spatial variation in the MW foreground since any M33 halo component, if present, is likely to be very weak. The number of stars in each annulus, and the number of stars within each of the three selection regions, are shown in Table 1.

4.1.   Extended Disk Substructure

Figure 3 is a revised version of Figure 13 in McConnachie et al. (2010), using the new data in images tb62-tb66 (see Figure 1). The map was created in an identical way to McConnachie et al. (see their Section 3.2.2 for details). Figure 3 shows the density contours of candidate RGB stars, and uses a slightly narrower metallicity cut of -2.0 dex $< [Fe/H] < $ -1.0 dex than the cut we impose on the candidate RGB stars in the CMDs. This narrower cut is used simply because this is the metallicity range in which the extended disk substructure component is strongest. There is hardly any contribution to the extended

disk substructure from stars with metallicity between -2.5 dex $< [Fe/H] <$ -2.0 dex; however, we would not necessarily expect this to be true of M33's halo RGB stars. The single grey contour represents 1σ above background, or an estimated surface brightness limit of $\mu_V = 33.0$ mag arcsec^{-2}. The other (black) contours are 2, 5, 8 and 12σ above the background ($\mu_V = 32.5, 31.7, 31.2,$ and 30.6 mag arcsec^{-2}, respectively).

Figure 4 shows the contributions to the total radial profile from the regions defined both within and excluding the 1σ contour shown in Figure 3. The profiles for the extended disk substructure and non-substructure regions are normalized using the total annulus area. The non-substructure regions are seen to start dominating the profile for $r > 2$ degrees. We exclude data within the 1σ contour when probing for the stellar halo. When we excise the extended disk substructure area denoted by the 1σ contour, note that we cannot probe radii smaller than $r \lesssim 1$ degree.

4.2.   Foreground and Background Contamination

We have identified candidate stars for the M33 RGB, and MW disk and halo populations, and we have identified the regions associated with the extended disk substructure surrounding the disk. We now test the populations for variations in the spatial distributions. Figure 5 shows smoothed non-excised maps of the spatial distribution for the background galaxies and each of the three populations identified in Figure 2 (i.e., the MW disk, MW halo and the M33 RGB candidate stars). We identify background galaxies morphologically using the CASU pipeline, and those shown in Figure 5 have had broad colour and magnitude cuts applied ($17 < i_0 < 23.5$, $17 < g_0 < 23.5$, and $-2 < (g-i)_0 < 4$).

The data is binned into 18 x 18 arcsecond cells. The galaxy, disk and halo maps are smoothed once, and the RGB map is smoothed three times, all with a boxcar size

of 13 x 13 cells (or equivalently 3.9 x 3.9 arcminutes; exactly four times smaller than in McConnachie et al. 2010). The RGB map is smoothed three times to better highlight the faint extended disk substructure surrounding the disk.

The galaxy, MW disk and MW halo maps clearly show no significant global features, although the centre of M33 is apparent due to the crowded nature in this region where the automated object morphological classification is less successful. Apparent holes in the data are caused by bright foreground stars preventing detection of faint objects in their surroundings. The galaxies misidentified as stars in our sample are expected to have a similar distribution to the galaxies shown in the galaxy map. The RGB map shows the extended substructure surrounding M33's disk, and Andromeda II to the north-west.

Now we excise the regions associated with the extended disk substructure surrounding the disk and investigate the variations of the MW disk and MW halo populations in different regions on the CMD within the 3-3.75 degree annulus (in which we expect little contribution from bona-fide M33 stars).

Figure 6 shows the variation of these three populations with respect to the azimuthal (left-hand column) and Galactic latitudinal (right-hand column) distributions. All panels show the variation between $3 < r \leq 3.75$ degrees, with extended disk substructure regions excised. Each of the three rows shows the density variation of M33 RGB, MW disk and MW halo candidate stars. The density of disk stars increases towards the disk, as does the density of the stars in the MW-halo selection region but with a smaller amplitude. As we do not expect the halo stars to vary in latitude in this manner, this suggests some cross-contamination with the thick disk stars.

Within the RGB selection shown in Figure 6, there is little variation in the annulus at large radii. Indeed, the best fit weighted least-squares fit in both RGB panels is consistent with a slope of zero. As such, we conclude that there is no reason to adopt a

spatially-varying foreground for our analysis, and instead use a constant background, Σ_{bg}.

4.3. Radial Profile

Having determined the extended disk substructure area to avoid, we produce substructure-excised radial profiles. As previously stated, we expect M33's halo to be extremely faint and centrally-concentrated so we bin the data in annuli centred on M33, where we require a certain signal-to-noise ratio for the bins in each profile.

Figure 7 shows radial density profiles of the RGB stars after excising extended disk substructure regions. The small vertical radial density error bars are calculated using $\sqrt{n}$/area as the error on the mean of the star counts in each stellar population. The horizontal error bars indicate the width of the annulus. The size of the annulus was allowed to vary until the signal-to-noise reached the required value (where the "noise" is the radial density uncertainty). Each bin in Figure 7 has a signal-to-noise (S/N) cut of 25. We also use different S/N cuts, but later show that the results are statistically the same. The larger error bars shown in Figure 7 show the variation due to residual substructure. These latter errors were measured as the standard deviation of number counts between azimuthal bins (36 degrees in width) around a given radial annulus.

In all the radial profiles, we see evidence for a low-luminosity and centrally concentrated profile in M33's RGB stars, which is beyond the extended disk substructure surrounding the disk, and has not previously been seen. For illustrative purpose only, as this component is so faint and the error bars are large, we use a Levenberg-Marquardt least squares method to fit the following exponential model, as shown by the curved lines in Figure 7:

$$\Sigma(r) = \Sigma_0 exp\left(-\frac{r}{r_0}\right) + \Sigma_{bg}; \tag{1}$$

The data points are overlaid with the best fit, as shown by the curved dashed line. The horizontal dashed lines show the background level estimated by the fit. We also show the background-subtracted fit with the solid curved lines at the bottom of each panel, where the use of a constant background is justified in the previous section. Table 2 shows the parameters associated with each of the fits at different S/N cuts, including the S/N = 25 cut shown in Figure 7. As previously mentioned, although the parameters vary slightly for each different S/N cut used, they are statistically the same.

We also test the effect of raising the faint limit of the RGB selection criteria to $i_0 = 23.5$ from $i_0 = 24.0$ magnitudes. When we make the brighter magnitude cut we exclude more contamination - as we would expect - but we include proportionally less signal. The form of the radial profile is essentially the same, although less defined. We therefore continue the analysis using the $i_0 = 24.0$ cut.

We approximate an equivalent surface brightness scale by using the conversion between stars counts and surface brightness described in McConnachie et al. (2010) (specifically, for $n_{RGB} < 350$ stars degree^{-2} from their Figure 15). For details of this conversion, see McConnachie et al. (2010), but note that *the conversion is only an approximation*. The RGB stars in McConnachie et al. are selected using -2 < [Fe/H] < -1 dex, and $i_0 < 23.5$ magnitudes, whereas here we use -2.5 < [Fe/H] < -1 dex, and $i_0 < 24.0$ magnitudes. There are also large systematic uncertainties inherent in the technique.

We estimate the luminosity of this component by first simply summing the total number of stars contributing to the profile in the radial range for which we have data (i.e., $0.88 \leq r \leq 3.75$ degrees), and using the conversion as above. Assuming Poisson statistics, we obtain 765 ± 95 stars (assuming a background of 355 stars degree^{-2}, and without propagating the uncertainty in the background), corresponding to a luminosity of $L = 2.4 \pm 0.4$ x $10^6 L_\odot$. Note that this initial estimate is independent of any assumptions we could

make about the profile of the component.

To calculate the luminosity extrapolated to the center, however, we assume a spherically symmetric smooth profile that is described by the exponential fit with a scale length of 1.5 degrees (or 21.1 kpc). We calculate the fraction of the integral of the exponential fit between $0.88 \leq r \leq 3.75$ degrees compared to $0 \leq r \leq 0.88$ degrees, allowing us to calculate the luminosity between $0 \leq r \leq 3.75$ degrees. This simple extrapolation yields an estimate of $L = 3.8 \pm 0.5$ x $10^6 L_\odot$. (If we use a similar technique to extrapolate under the whole exponential curve, i.e., out to infintiy, we obtain $L = 4.1 \pm 0.5$ x $10^6 L_\odot$.) We note that the large uncertainties on the exponential profile fit to our data and the unknown intrinsic profile of this component, make these extrapolated estimates highly uncertain. As noted above, we also do not include the error on the background. The effect of including this is seen in Figure 8; as we integrate out to larger radii, the relative luminosity error estimates increase. At larger radii, there are fewer candidate RGB stars but a relatively larger contribution from the background.

5. Discussion and Conclusions

It was expected that any stellar halo signal around M33 would be at least as faint as the recently discovered extended optical disk substructure surrounding the disk (McConnachie et al. 2009, 2010). Hints of a radial fall off beyond the extent of the extended disk substructure suggested a tentative halo detection (McConnachie et al. 2010). We followed up this possibility in our present study, using higher spatial resolution maps, excising any contribution from the extended disk substructure, and subtracting off contamination from foreground and background sources, so that we are more able to cleanly resolve and identify any remaining signal.

We detect a radial density drop off that we interpret as an upper limit of the M33 candidate stellar halo. The signal is extremely faint, but seems robust to various signal-to-noise cuts; as previously noted, we observe only 765 ± 95 excess stars between $0.88 < r < 3.75$ degrees.

Are we justified in claiming this extra component is a halo? We have azimuthally averaged annuli centred on M33 to find a low-luminosity and centrally concentrated profile. The top panel of Figure 9 shows the azimuthal distribution of the RGB candidate star density within 3 degrees having excised the extended disk substructure regions. We see contamination of the MW foreground stars does not appear to affect the density variation of these RGB candidate stars (i.e., we do not see a reflection of the density profiles shown in Figure 6 for the MW disk candidate stars). If our extra component was actually residual low-level emission from the already known extended disk substructure we would expect to see this reflected in this plot, with overdensities around the regions associated with the tips of the S-shaped warp, indicated by the two arrows in the top panel. The azimuthal distribution is fairly flat, but we note that overdensities are apparent near the warp's tips suggesting some contamination from the extended disk substructure. We further split the data into two annuli, 1-2 and 2-3 degrees, but we do not see evidence that the RGB candidates show any major differences in their azimuthal distribution from one another in either annulus.

Further constraining this newly discovered component, we show in Figure 10 the CMD for all objects with $r < 3$ degrees, except for those within the extended disk substructure's 1σ contours in Figure 3 (again, this imposes a minimum radius of $\sim$1 degree). We note that the RGB stars that we aim to detect are just visible to the eye on the left-hand plot. Again, we see the extreme relative faintness of this component. On the middle panel we overlay an [Fe/H] = -2 dex isochrone to this feature. As expected if this component is a

halo, this crude measurement indicates that it is relatively metal-poor. The extended disk substructure metallicity for comparison is [Fe/H] = -1.6 dex (McConnachie et al. 2010). We show the CMD for the extended disk substructure in the right-hand panel, again overlaying an [Fe/H] = -2 dex isochrone for comparison. We can see that the candidate halo lies on the metal-poor side of the extended disk substructure RGB.

With this component that we identify as M33's candidate halo, it is appropriate to ask - even with such poor signal-to-noise - if we see any azimuthal asymmetry. To test for this, we split the data into the four quadrants split by the major and minor axes, e.g., as shown in Figure 3. The resulting radial profiles for each quadrant are shown in Figure 11, and the associated CMDs are shown in Figure 12. It appears as if the east and south quadrants have the steepest radial declines, whereas the north and west quadrants are flatter. In other words, there may be a variation in the radial profile of the candidate halo when split along the major axis. Further interpretation of this possible asymmetry must wait for higher quality and deeper data.

In summary, we have a weak detection that is not clearly indistinguishable in either azimuthal distribution or metallicity from the extended disk substructure component. If this is a halo, we use the estimates so far obtained to place upper limits on the luminosity. We note that with the data at hand we must leave open that it could be another component, such as a very extended thick disk.

The location of the extended disk substructure was the most important knowledge prior to beginning this study, in a similar way that the spectroscopic knowledge of the metal-rich component led to the discovery of the metal-poor halo in M31 (Chapman et al. 2006; Kalirai et al. 2006). If we directly compare M31's halo with M33's candidate halo we find that apart from the obvious difference in luminosity ($L_{M31,halo,V} \sim 10^9 L_{\odot}$, Ibata et al. 2007; $L_{M33,halo,V} = 4.1 \pm 0.5$ x $10^6 L_{\odot}$.), expected because of the mass difference between the two

galaxies, it is unclear if the exponential scale lengths are significantly different; we estimate M33's scale length to be 21 ± 18 kpc, similar to that found for M31 (~ 14 kpc; Irwin et al. 2005). In light of the discovery here, the spectroscopic work by McConnachie et al. (2006) needs to be revisited so that a comparison of M31 and M33's halo metallicity can be made (see Trethewey 2011, and a forthcoming paper by Trethewey et al. 2012).

As mentioned in Section 2.4, the favoured interpretation to explain M33's extended disk substructure surrounding the disk is a tidal interaction with M31 (McConnachie et al. 2009, 2010). It is extremely likely that this interaction also affected M33's halo: at least altering if not stripping it, with some of M33's halo then being accreted onto M31. The halo could also extend beyond the point to which the PAndAS data set is able to measure it (~ 3.75 degrees, or ~ 5 degrees to the north-east.) In the supplementary material movie of McConnachie et al. (2009), the end of the modelled interaction also includes the stellar halo. Though a significant amount of halo material is stripped from M33, appearing to extend beyond the virial radius to form a low-luminosity bridge between M33 and M31, most of the halo appears to remain bound to M33. The material stripped from M33's halo also extends well beyond the area observed in PAndAS. More of the remaining bound material appears on the south-east side (away from M31) than in the north-west (closest to M31). Our observations appear to broadly agree with this model, as we see more of a gradient in the radial profile in the south quadrant.

The most probable scenario(s) for how M33's candidate halo was built could be quite different from Milky Way and M31 because it is approximately ten times less massive than either. Unlike M31, M33 has no bulge, a warped extended disk substructure, and is likely interacting with a much more massive neighbour. Studies of the M33 outer halo clusters also suggest that with the low GC surface density ($\Sigma_{GC,M33} \sim 0.14$ deg^{-2}) compared to M31 ($\Sigma_{GC,M31} \sim 0.8$ deg^{-2}), M33 either had a much calmer accretion history than M31 or

that some of the outer halo clusters could have been tidally stripped by M31 (Huxor et al. 2009; Cockcroft et al. 2011). The latter idea obviously supports the favoured interpretation that could explain the warped extended disk substructure component.

We now compare our results with a model that predicts the size of M33's stellar halo. Purcell et al. (2007) use an analytic model with empirical constraints from $z \sim 0$ observations to predict the fraction of stellar halo mass compared to the total luminous mass. They define the diffuse stellar mass fraction as $f_{IHL} = M_*^{diff}/M_*^{total}$; note that they use mass rather than luminosities, to avoid uncertainties involved with luminosity evolution. There is no distinction made between the substructure in the halo, or the smooth diffuse halo that might underlie the substructure. Their predictions cover a range of host galaxy's dark matter halo masses, from small late-type galaxies to large galaxy clusters ($\sim 10^{11}$ to $\sim 10^{15}$ $M_\odot$). The stellar material is assumed to be able to become part of the diffuse stellar halo when its dark matter subhalo has become significantly stripped. The dark matter subhalo is considered disrupted when its maximum circular velocity falls below a critical value - which is set by considering the empirical constraints. For DM halos of mass $\sim 10^{11} M_\odot$ ($\sim M_{M33}$; Corbelli & Salucci 2000), the stellar halo luminosity fraction is expected to be $\leq 1.0\%$ (thus, $L_{stellarhalo} \leq 10^7 L_\odot$). A galaxy's mass-to-light ratio (over the entire halo out to the virial radius) varies as a function of DM halo mass, and this drives the fraction of stellar halo material; small galaxies are expected to accrete material from dwarf galaxies, which have high mass-to-light ratios and therefore share little luminous material with their host galaxy's stellar halo (Purcell et al. 2007). Even if they share all of their material, the contribution is not large. This picture seems to broadly agree with our upper limit estimate of M33's extremely faint candidate stellar halo, $L_{M33,halo,V} = 4.1 \pm 0.5$ x $10^6 L_\odot$ ($0.4\% \lesssim L_{M33,host,V} \lesssim 0.5\%$).

Figure 13 plots the fraction of halo luminosity compared to the host galaxy luminosity,

against the host galaxy mass for several galaxies including M33. The lines represent equation 7 from Purcell et al. (2007) for the model of the intrahalo light, with different values for the parameters n_{eff} and f_d. Here, n_{eff}, expected to be of order unity, represents the effective number of satellites with mass $M_{sat} = M_{host}/20$; f_d represents the total stellar mass fraction a satellite contributes to its host galaxy halo. We note that if we swap the values for f_d and n_{eff}, the lines would vary in the same way.

The two estimates for M33's candidate halo luminosity fraction are for the directly observed estimate ($0.88 < r < 3.75$ degrees), and the implied, extrapolated estimate ($r < 10.64$ degrees). The values for the MW and M31 are taken from Sections 2.1 and 2.2, respectively. We also include estimates of the NGC 2403's extended component (Barker et al. 2012), as it has a similar total stellar mass to M33 (9.4 ± 0.7 x $10^{10} M_\odot$; Fraternali et al. 2002). It is at a distance of 3.1 Mpc (Freedman et al. 2001), has an inclination of 63 degrees (Fraternali et al. 2002), and is the brightest member of a loose galaxy group and is therefore considered much more isolated than M33 (the closest large galaxy is M81, which is four times further from NGC 2403 than M33 is from M31; Barker et al. 2012). Barker et al. use Subaru/Suprime-Cam to obtain images 39 x 48 kpc around the centre of NGC 2403, and see an extended component which could be disk structure or a halo. Extrapolating out to 50 kpc they find that the haloes contain $\sim$ 1-7 % of the total V-band luminosity, or $L_{2403,halo,V} \sim$ 1-7 x $10^8 L_\odot$, depending on whether or not an exponential or Hernquist profile is used (if they extrapolate out to 100 kpc the estimate does not significantly change).

The values of $L_{halo}/L_{hostgalaxy}$ for the MW and M31 are close to those of the models by Purcell et al. (2007). However, for the less massive galaxy NGC 2403 we find the models seem to underestimate the contribution of halo light from these smaller galaxies - and may also do the same for M33, although with such a weak signal as we detect here there are

large uncertainties. If we further include M33's extended disk substructure ($L_{substructure} \sim 10^7 L_\odot$) in the "halo" term, we see that M33 lies even further from the model lines. How do we interpret this information? A value of $f_d = 1$ implies that any satellite galaxy has been completely destroyed and contributed all of its material to the halo. The MW and M31 data seem to favour a value of $f_d = 1$, which is of course inconsistent with observations (e.g., M31's latest tally is up to 29; Richardson et al. 2011, Slater et al. 2011, Bell et al. 2011). If the M33 candidate halo fraction is closer to the upper bounds, then it also appears that the models underestimate the halo fraction for lower-luminosity galaxies.

6.   Summary

We use Pan-Andromeda Archaeological Survey (PAndAS) data to identify RGB candidate stars in the regions unrelated to the disk and extended disk substructure surrounding the disk. Contamination from both Milky Way foreground stars and misidentified background galaxies is subtracted. We reveal a new component centred on M33 that has a low luminosity. With such a weak signal, measurements are not well constrained by our data. However, it appears that this component has an exponential scale length is of order $r_{exp} \sim 20$ kpc, a photometric metallicity of around [Fe/H] $\sim$ -2 dex, a luminosity range of a few percent of M33's total host luminosity, and is azimuthally asymmetric. More observations and deeper photometry are required to better determine the detailed structure of the stellar populations.

If this feature is truly a halo, it provides support that stellar halos are a ubiquitous component of all galaxies, built through the hierarchical merging predicted in ΛCDM cosmology.

REFERENCES

Alves, D. R. 2004, ApJ, 601, L151

Athanassoula, E., & Beaton, R. L. 2006, MNRAS, 370, 1499

Baiesi Pillastrini, G. C. 2009, MNRAS, 397, 1990

Bailin, J., Bell, E. F., Chappell, S. N., Radburn-Smith, D. J., & de Jong, R. S. 2011, ApJ, 736, 24

Barker, M. K., Ferguson, A. M. N., Cole, A. A., Ibata, R., Irwin, M., Lewis, G. F., Smecker-Hane, T. A., & Tanvir, N. R. 2011, MNRAS, 410, 504

Barker, M. K., Ferguson, A. M. N., Irwin, M., Arimoto, N., & Jablonka, P. 2009, AJ, 138, 1469

Barker, M. K., Ferguson, A. M. N., Irwin, M. J., Arimoto, N., & Jablonka, P. 2012, MNRAS, 419, 1489

Barker, M. K., Sarajedini, A., Geisler, D., Harding, P., & Schommer, R. 2007a, AJ, 133, 1125

—. 2007b, AJ, 133, 1138

Beers, T. C., Carollo, D., Ivezić, Ž., An, D., Chiba, M., Norris, J. E., Freeman, K. C., Lee, Y. S., Munn, J. A., Re Fiorentin, P., Sivarani, T., Wilhelm, R., Yanny, B., & York, D. G. 2012, ApJ, 746, 34

Bekki, K. 2007, MNRAS, 380, 1669

Bekki, K., & Stanimirović, S. 2009, MNRAS, 395, 342

Bell, E. F., Slater, C. T., & Martin, N. F. 2011, ApJ, 742, L15

Bell, E. F., Zucker, D. B., Belokurov, V., Sharma, S., Johnston, K. V., Bullock, J. S., Hogg, D. W., Jahnke, K., de Jong, J. T. A., Beers, T. C., Evans, N. W., Grebel, E. K., Ivezić, Ž., Koposov, S. E., Rix, H.-W., Schneider, D. P., Steinmetz, M., & Zolotov, A. 2008, ApJ, 680, 295

Belokurov, V., Evans, N. W., Bell, E. F., Irwin, M. J., Hewett, P. C., Koposov, S., Rockosi, C. M., Gilmore, G., Zucker, D. B., Fellhauer, M., Wilkinson, M. I., Bramich, D. M., Vidrih, S., Rix, H.-W., Beers, T. C., Schneider, D. P., Barentine, J. C., Brewington, H., Brinkmann, J., Harvanek, M., Krzesinski, J., Long, D., Pan, K., Snedden, S. A., Malanushenko, O., & Malanushenko, V. 2007a, ApJ, 657, L89

Belokurov, V., Evans, N. W., Irwin, M. J., Lynden-Bell, D., Yanny, B., Vidrih, S., Gilmore, G., Seabroke, G., Zucker, D. B., Wilkinson, M. I., Hewett, P. C., Bramich, D. M., Fellhauer, M., Newberg, H. J., Wyse, R. F. G., Beers, T. C., Bell, E. F., Barentine, J. C., Brinkmann, J., Cole, N., Pan, K., & York, D. G. 2007b, ApJ, 658, 337

Belokurov, V., Zucker, D. B., Evans, N. W., Gilmore, G., Vidrih, S., Bramich, D. M., Newberg, H. J., Wyse, R. F. G., Irwin, M. J., Fellhauer, M., Hewett, P. C., Walton, N. A., Wilkinson, M. I., Cole, N., Yanny, B., Rockosi, C. M., Beers, T. C., Bell, E. F., Brinkmann, J., Ivezić, Ž., & Lupton, R. 2006, ApJ, 642, L137

Bergvall, N., Zackrisson, E., & Caldwell, B. 2010, MNRAS, 405, 2697

Bonanos, A. Z., Stanek, K. Z., Kudritzki, R. P., Macri, L. M., Sasselov, D. D., Kaluzny, J., Stetson, P. B., Bersier, D., Bresolin, F., Matheson, T., Mochejska, B. J., Przybilla, N., Szentgyorgyi, A. H., Tonry, J., & Torres, G. 2006, ApJ, 652, 313

Bothun, G. D. 1992, AJ, 103, 104

Brunthaler, A., Reid, M. J., Falcke, H., Greenhill, L. J., & Henkel, C. 2005, Science, 307, 1440

Buehler, S., Ferguson, A. M. N., Irwin, M. J., Arimoto, N., & Jablonka, P. 2007, in IAU Symposium, Vol. 241, IAU Symposium, ed. A. Vazdekis & R. F. Peletier, 321–322

Bullock, J. S., & Johnston, K. V. 2005, ApJ, 635, 931

Carney, B. W., Latham, D. W., & Laird, J. B. 1990, AJ, 99, 572

Carollo, D., Beers, T. C., Lee, Y. S., Chiba, M., Norris, J. E., Wilhelm, R., Sivarani, T., Marsteller, B., Munn, J. A., Bailer-Jones, C. A. L., Fiorentin, P. R., & York, D. G. 2007, Nature, 450, 1020

Chandar, R., Bianchi, L., & Ford, H. C. 2001, A&A, 366, 498

Chandar, R., Bianchi, L., Ford, H. C., & Sarajedini, A. 2002, ApJ, 564, 712

Chapman, S. C., Ibata, R., Lewis, G. F., Ferguson, A. M. N., Irwin, M., McConnachie, A., & Tanvir, N. 2006, ApJ, 653, 255

Chiba, M., & Beers, T. C. 2000, AJ, 119, 2843

Cioni, M., Irwin, M., Ferguson, A. M. N., McConnachie, A., Conn, B. C., Huxor, A., Ibata, R., Lewis, G., & Tanvir, N. 2008, A&A, 487, 131

Cockcroft, R., Harris, W. E., Ferguson, A. M. N., Huxor, A., Ibata, R., Irwin, M. J., McConnachie, A. W., Woodley, K. A., Chapman, S. C., Lewis, G. F., & Puzia, T. H. 2011, ApJ, 730, 112

Conn, A. R., Ibata, R. A., Lewis, G. F., Parker, Q. A., & B., Z. D. 2012, ApJ, in prep

Corbelli, E., Magrini, L., & Verley, S. 2008, in Astronomical Society of the Pacific Conference Series, Vol. 396, Formation and Evolution of Galaxy Disks, ed. J. G. Funes & E. M. Corsini, 19–+

Corbelli, E., & Salucci, P. 2000, MNRAS, 311, 441

Courteau, S., Widrow, L. M., McDonald, M., Guhathakurta, P., Gilbert, K. M., Zhu, Y., Beaton, R. L., & Majewski, S. R. 2011, ApJ, 739, 20

Crane, J. D., Majewski, S. R., Rocha-Pinto, H. J., Frinchaboy, P. M., Skrutskie, M. F., & Law, D. R. 2003, ApJ, 594, L119

Crotts, A. P. S. 1986, AJ, 92, 292

Dalcanton, J. J., & Bernstein, R. A. 2002, AJ, 124, 1328

de Jong, J. T. A., Yanny, B., Rix, H.-W., Dolphin, A. E., Martin, N. F., & Beers, T. C. 2010, ApJ, 714, 663

de Jong, R. S. 2008, MNRAS, 388, 1521

de Jong, R. S., Radburn-Smith, D. J., & Sick, J. N. 2008, in Astronomical Society of the Pacific Conference Series, Vol. 396, Formation and Evolution of Galaxy Disks, ed. J. G. Funes & E. M. Corsini, 187

de Jong, R. S., Seth, A. C., Radburn-Smith, D. J., Bell, E. F., Brown, T. M., Bullock, J. S., Courteau, S., Dalcanton, J. J., Ferguson, H. C., Goudfrooij, P., Holfeltz, S., Holwerda, B. W., Purcell, C., Sick, J., & Zucker, D. B. 2007, ApJ, 667, L49

de Vaucouleurs, G. 1959, ApJ, 130, 728

de Vaucouleurs, G., de Vaucouleurs, A., Corwin, Jr., H. G., Buta, R. J., Paturel, G., & Fouque, P. 1991, Third Reference Catalogue of Bright Galaxies (New York: Springer-Verlag)

Deason, A. J., Belokurov, V., & Evans, N. W. 2011, MNRAS, 416, 2903

Dotter, A., Chaboyer, B., Jevremović, D., Baron, E., Ferguson, J. W., Sarajedini, A., & Anderson, J. 2007, AJ, 134, 376

Dotter, A., Chaboyer, B., Jevremović, D., Kostov, V., Baron, E., & Ferguson, J. W. 2008, ApJS, 178, 89

Dubinski, J., Widrow, L., W., M. A., R., I., & et al., I. M. J. in prep., ApJ

Dubus, G., Long, K. S., & Charles, P. A. 1999, ApJ, 519, L135

Evans, N. W., & Wilkinson, M. I. 2000, MNRAS, 316, 929

Ferguson, A., Irwin, M., Chapman, S., Ibata, R., Lewis, G., & Tanvir, N. 2007, Resolving the Stellar Outskirts of M31 and M33 (Island Universes: Berlin: Springer), 239–+

Ferguson, A. M. N. 2007, in Astronomical Society of the Pacific Conference Series, Vol. 374, From Stars to Galaxies: Building the Pieces to Build Up the Universe, ed. A. Vallenari, R. Tantalo, L. Portinari, & A. Moretti, 239

Ferguson, A. M. N., Irwin, M. J., Ibata, R. A., Lewis, G. F., & Tanvir, N. R. 2002, AJ, 124, 1452

Foschini, L., Rodriguez, J., Fuchs, Y., Ho, L. C., Dadina, M., Di Cocco, G., Courvoisier, T. J.-L., & Malaguti, G. 2004, A&A, 416, 529

Fraternali, F., van Moorsel, G., Sancisi, R., & Oosterloo, T. 2002, AJ, 123, 3124

Freedman, W. L., Madore, B. F., Gibson, B. K., Ferrarese, L., Kelson, D. D., Sakai, S., Mould, J. R., Kennicutt, Jr., R. C., Ford, H. C., Graham, J. A., Huchra, J. P., Hughes, S. M. G., Illingworth, G. D., Macri, L. M., & Stetson, P. B. 2001, ApJ, 553, 47

Freeman, K. C., Illingworth, G., & Oemler, Jr., A. 1983, ApJ, 272, 488

Grillmair, C. J. 2006, ApJ, 645, L37

Grossi, M., Hwang, N., Corbelli, E., Giovanardi, C., Okamoto, S., & Arimoto, N. 2011, A&A, 533, A91

Harris, W. E., Harris, G. L. H., Layden, A. C., & Wehner, E. M. H. 2007, ApJ, 666, 903

Helmi, A. 2008, A&A Rev., 15, 145

Huxor, A., Ferguson, A. M. N., Barker, M. K., Tanvir, N. R., Irwin, M. J., Chapman, S. C., Ibata, R., & Lewis, G. 2009, ApJ, 698, L77

Ibata, R., Chapman, S., Ferguson, A. M. N., Irwin, M., Lewis, G., & McConnachie, A. 2004, MNRAS, 351, 117

Ibata, R., Chapman, S., Ferguson, A. M. N., Lewis, G., Irwin, M., & Tanvir, N. 2005, ApJ, 634, 287

Ibata, R., Irwin, M., Lewis, G., Ferguson, A. M. N., & Tanvir, N. 2001a, Nature, 412, 49

Ibata, R., Irwin, M., Lewis, G. F., & Stolte, A. 2001b, ApJ, 547, L133

Ibata, R., Martin, N. F., Irwin, M., Chapman, S., Ferguson, A. M. N., Lewis, G. F., & McConnachie, A. W. 2007, ApJ, 671, 1591

Ibata, R. A., Gilmore, G., & Irwin, M. J. 1994, Nature, 370, 194

Ibata, R. A., Irwin, M. J., Lewis, G. F., Ferguson, A. M. N., & Tanvir, N. 2003, MNRAS, 340, L21

Ibata, R. A., Lewis, G. F., Irwin, M. J., & Cambrésy, L. 2002, MNRAS, 332, 921

Irwin, M., & Lewis, J. 2001, New Astronomy Reviews, 45, 105

Irwin, M. J., Ferguson, A. M. N., Ibata, R. A., Lewis, G. F., & Tanvir, N. R. 2005, ApJ, 628, L105

Javadi, A., van Loon, J. T., & Mirtorabi, M. T. 2011, MNRAS, 414, 3394

Johnston, K. V., Hernquist, L., & Bolte, M. 1996, ApJ, 465, 278

Jurić, M., Ivezić, Ž., Brooks, A., Lupton, R. H., Schlegel, D., Finkbeiner, D., Padmanabhan, N., Bond, N., Sesar, B., Rockosi, C. M., Knapp, G. R., Gunn, J. E., Sumi, T., Schneider, D. P., Barentine, J. C., Brewington, H. J., Brinkmann, J., Fukugita, M., Harvanek, M., Kleinman, S. J., Krzesinski, J., Long, D., Neilsen, Jr., E. H., Nitta, A., Snedden, S. A., & York, D. G. 2008, ApJ, 673, 864

Kalirai, J. S., Gilbert, K. M., Guhathakurta, P., Majewski, S. R., Ostheimer, J. C., Rich, R. M., Cooper, M. C., Reitzel, D. B., & Patterson, R. J. 2006, ApJ, 648, 389

Koch, A., Rich, R. M., Reitzel, D. B., Martin, N. F., Ibata, R. A., Chapman, S. C., Majewski, S. R., Mori, M., Loh, Y.-S., Ostheimer, J. C., & Tanaka, M. 2008, ApJ, 689, 958

Kormendy, J., Drory, N., Bender, R., & Cornell, M. E. 2010, ApJ, 723, 54

Law, D. R., & Majewski, S. R. 2010, ApJ, 714, 229

Law, D. R., Majewski, S. R., & Johnston, K. V. 2009, ApJ, 703, L67

Long, K. S., Dodorico, S., Charles, P. A., & Dopita, M. A. 1981, ApJ, 246, L61

Majewski, S. R., Nidever, D. L., Muñoz, R. R., Patterson, R. J., Kunkel, W. E., & Carlin, J. L. 2009, in IAU Symposium, Vol. 256, IAU Symposium, ed. J. T. van Loon & J. M. Oliveira, 51–56

Majewski, S. R., Skrutskie, M. F., Weinberg, M. D., & Ostheimer, J. C. 2003, ApJ, 599, 1082

Malin, D. F., Quinn, P. J., & Graham, J. A. 1983, ApJ, 272, L5

Martin, N. F., Ibata, R. A., Bellazzini, M., Irwin, M. J., Lewis, G. F., & Dehnen, W. 2004a, MNRAS, 348, 12

Martin, N. F., Ibata, R. A., Conn, B. C., Lewis, G. F., Bellazzini, M., Irwin, M. J., & McConnachie, A. W. 2004b, MNRAS, 355, L33

Martin, N. F., Ibata, R. A., & Irwin, M. 2007, ApJ, 668, L123

Martin, N. F., McConnachie, A. W., Irwin, M., Widrow, L. M., Ferguson, A. M. N., Ibata, R. A., Dubinski, J., Babul, A., Chapman, S., Fardal, M., Lewis, G. F., Navarro, J., & Rich, R. M. 2009, ApJ, 705, 758

Martínez-Delgado, D., Gabany, R. J., Crawford, K., Zibetti, S., Majewski, S. R., Rix, H.-W., Fliri, J., Carballo-Bello, J. A., Bardalez-Gagliuffi, D. C., Peñarrubia, J., Chonis, T. S., Madore, B., Trujillo, I., Schirmer, M., & McDavid, D. A. 2010, AJ, 140, 962

McCarthy, I. G., Font, A. S., Crain, R. A., Deason, A. J., Schaye, J., & Theuns, T. 2012, MNRAS, 420, 2245

McConnachie, A. W., Chapman, S. C., Ibata, R. A., Ferguson, A. M. N., Irwin, M. J., Lewis, G. F., Tanvir, N. R., & Martin, N. 2006, ApJ, 647, L25

McConnachie, A. W., Ferguson, A. M. N., Irwin, M. J., Dubinski, J., Widrow, L. M., Dotter, A., Ibata, R., & Lewis, G. F. 2010, ApJ, 723, 1038

McConnachie, A. W., Irwin, M. J., Ferguson, A. M. N., Ibata, R. A., Lewis, G. F., & Tanvir, N. 2004, MNRAS, 350, 243

—. 2005, MNRAS, 356, 979

McConnachie, A. W., Irwin, M. J., Ibata, R. A., Dubinski, J., Widrow, L. M., Martin, N. F., Côté, P., Dotter, A. L., Navarro, J. F., Ferguson, A. M. N., Puzia, T. H., Lewis, G. F., Babul, A., Barmby, P., Bienaymé, O., Chapman, S. C., Cockcroft, R., Collins, M. L. M., Fardal, M. A., Harris, W. E., Huxor, A., Mackey, A. D., Peñarrubia, J., Rich, R. M., Richer, H. B., Siebert, A., Tanvir, N., Valls-Gabaud, D., & Venn, K. A. 2009, Nature, 461, 66

McLean, I. S., & Liu, T. 1996, ApJ, 456, 499

Miceli, A., Rest, A., Stubbs, C. W., Hawley, S. L., Cook, K. H., Magnier, E. A., Krisciunas, K., Bowell, E., & Koehn, B. 2008, ApJ, 678, 865

Minniti, D., Borissova, J., Rejkuba, M., Alves, D. R., Cook, K. H., & Freeman, K. C. 2003, Science, 301, 1508

Minniti, D., Olszewski, E. W., & Rieke, M. 1993, ApJ, 410, L79

Mouhcine, M., Ibata, R., & Rejkuba, M. 2010, ApJ, 714, L12

Mouhcine, M., Rejkuba, M., & Ibata, R. 2007, MNRAS, 381, 873

Mould, J., & Kristian, J. 1986, ApJ, 305, 591

Newberg, H. J., & Yanny, B. 2006, Journal of Physics Conference Series, 47, 195

Newberg, H. J., Yanny, B., Rockosi, C., Grebel, E. K., Rix, H., Brinkmann, J., Csabai, I., Hennessy, G., Hindsley, R. B., Ibata, R., Ivezić, Z., Lamb, D., Nash, E. T., Odenkirchen, M., Rave, H. A., Schneider, D. P., Smith, J. A., Stolte, A., & York, D. G. 2002, ApJ, 569, 245

Newberg, H. J., Yanny, B., & Willett, B. A. 2009, ApJ, 700, L61

Nidever, D. L., Majewski, S. R., Muñoz, R. R., Beaton, R. L., Patterson, R. J., & Kunkel, W. E. 2011, ApJ, 733, L10

Nilson, P. 1973, Nova Acta Regiae Soc. Sci. Upsaliensis Ser. V, 0

Oser, L., Ostriker, J. P., Naab, T., Johansson, P. H., & Burkert, A. 2010, ApJ, 725, 2312

Peng, E. W., Ford, H. C., Freeman, K. C., & White, R. L. 2002, AJ, 124, 3144

Purcell, C. W., Bullock, J. S., & Zentner, A. R. 2007, ApJ, 666, 20

Putman, M. E., Peek, J. E. G., Muratov, A., Gnedin, O. Y., Hsu, W., Douglas, K. A., Heiles, C., Stanimirovic, S., Korpela, E. J., & Gibson, S. J. 2009, ApJ, 703, 1486

Radburn-Smith, D. J., de Jong, R. S., Seth, A. C., Bailin, J., Bell, E. F., Brown, T. M., Bullock, J. S., Courteau, S., Dalcanton, J. J., Ferguson, H. C., Goudfrooij, P., Holfeltz, S., Holwerda, B. W., Purcell, C., Sick, J., Streich, D., Vlajic, M., & Zucker, D. B. 2011, ApJS, 195, 18

Rejkuba, M., Harris, W. E., Greggio, L., & Harris, G. L. H. 2011, A&A, 526, A123

Rejkuba, M., Mouhcine, M., & Ibata, R. 2009, MNRAS, 396, 1231

Rich, R. M., Collins, M. L. M., Black, C. M., Longstaff, F. A., Koch, A., Benson, A., & Reitzel, D. B. 2012, Nature, 482, 192

Richardson, J. C., Irwin, M. J., McConnachie, A. W., Martin, N. F., Dotter, A. L., Ferguson, A. M. N., Ibata, R. A., Chapman, S. C., Lewis, G. F., Tanvir, N. R., & Rich, R. M. 2011, ApJ, 732, 76

Rocha-Pinto, H. J., Majewski, S. R., Skrutskie, M. F., Crane, J. D., & Patterson, R. J. 2004, ApJ, 615, 732

Rogstad, D. H., Wright, M. C. H., & Lockhart, I. A. 1976, ApJ, 204, 703

Rubin, V. C., Ford, Jr., W. K., & Krishna Kumar, C. 1973, ApJ, 181, 61

Ryś, A., Grocholski, A. J., van der Marel, R. P., Aloisi, A., & Annibali, F. 2011, A&A, 530, A23

Sackett, P. D. 1997, ApJ, 483, 103

Sackett, P. D., Morrisoni, H. L., Harding, P., & Boroson, T. A. 1994, Nature, 370, 441

Sarajedini, A. 2007, in Revista Mexicana de Astronomia y Astrofisica Conference Series, Vol. 29, Revista Mexicana de Astronomia y Astrofisica Conference Series, ed. R. Guzmán, 48–50

Sarajedini, A., Barker, M. K., Geisler, D., Harding, P., & Schommer, R. 2006, AJ, 132, 1361

Schlaufman, K. C., Rockosi, C. M., Allende Prieto, C., Beers, T. C., Bizyaev, D., Brewington, H., Lee, Y. S., Malanushenko, V., Malanushenko, E., Oravetz, D., Pan, K., Simmons, A., Snedden, S., & Yanny, B. 2009, ApJ, 703, 2177

Schlaufman, K. C., Rockosi, C. M., Lee, Y. S., Beers, T. C., Allende Prieto, C., Rashkov, V., Madau, P., & Bizyaev, D. 2012, ApJ, 749, 77

Schlegel, D. J., Finkbeiner, D. P., & Davis, M. 1998, ApJ, 500, 525

Schommer, R. A., Suntzeff, N. B., Olszewski, E. W., & Harris, H. C. 1992, AJ, 103, 447

Seth, A., de Jong, R., Dalcanton, J., & GHOSTS Team. 2007, in IAU Symposium, Vol. 241, IAU Symposium, ed. A. Vazdekis & R. F. Peletier, 523–524

Shang, Z., Zheng, Z., Brinks, E., Chen, J., Burstein, D., Su, H., Byun, Y.-I., Deng, L., Deng, Z., Fan, X., Jiang, Z., Li, Y., Lin, W., Ma, F., Sun, W.-H., Wills, B., Windhorst,

R. A., Wu, H., Xia, X., Xu, W., Xue, S., Yan, H., Zhou, X., Zhu, J., & Zou, Z. 1998, ApJ, 504, L23

Slater, C. T., Bell, E. F., & Martin, N. F. 2011, ApJ, 742, L14

Tanaka, M., Chiba, M., Komiyama, Y., Guhathakurta, P., & Kalirai, J. S. 2011, ApJ, 738, 150

Teig, M. 2008, PASP, 120, 474

Tiede, G. P., Sarajedini, A., & Barker, M. K. 2004, AJ, 128, 224

Tikhonov, N. A., & Galazutdinova, O. A. 2005, Astrophysics, 48, 221

Trethewey, D. 2011, University of Cambridge: Masters dissertation

Trethewey, D., Chapman, S. C., Irwin, M. J., McConnachie, A. W., Lewis, G. F., Collins, M. L. M., Ferguson, A. M. N., Ibata, R., Rich, M., & Tanvir, N. 2012, in preparation

van den Bergh, S. 1999, A&A Rev., 9, 273

van der Marel, R. P., Alves, D. R., Hardy, E., & Suntzeff, N. B. 2002, AJ, 124, 2639

Venn, K. A., Irwin, M., Shetrone, M. D., Tout, C. A., Hill, V., & Tolstoy, E. 2004, AJ, 128, 1177

Vivas, A. K., Zinn, R., Andrews, P., Bailyn, C., Baltay, C., Coppi, P., Ellman, N., Girard, T., Rabinowitz, D., Schaefer, B., Shin, J., Snyder, J., Sofia, S., van Altena, W., Abad, C., Bongiovanni, A., Briceño, C., Bruzual, G., Della Prugna, F., Herrera, D., Magris, G., Mateu, J., Pacheco, R., Sánchez, G., Sánchez, G., Schenner, H., Stock, J., Vicente, B., Vieira, K., Ferrín, I., Hernandez, J., Gebhard, M., Honeycutt, R., Mufson, S., Musser, J., & Rengstorf, A. 2001, ApJ, 554, L33

Watkins, L. L., Evans, N. W., & An, J. H. 2010, MNRAS, 406, 264

Weil, M. L., Bland-Hawthorn, J., & Malin, D. F. 1997, ApJ, 490, 664

Xu, Y., Deng, L. C., & Hu, J. Y. 2006, MNRAS, 368, 1811

Yanny, B., Newberg, H. J., Grebel, E. K., Kent, S., Odenkirchen, M., Rockosi, C. M., Schlegel, D., Subbarao, M., Brinkmann, J., Fukugita, M., Ivezic, Ž., Lamb, D. Q., Schneider, D. P., & York, D. G. 2003, ApJ, 588, 824

Zackrisson, E., de Jong, R. S., & Micheva, G. 2011, ArXiv e-prints

Zackrisson, E., & Micheva, G. 2011, ArXiv e-prints

Zaritsky, D., Elston, R., & Hill, J. M. 1989, AJ, 97, 97

Zibetti, S., & Ferguson, A. M. N. 2004, MNRAS, 352, L6

Zibetti, S., White, S. D. M., & Brinkmann, J. 2004, MNRAS, 347, 556

Zolotov, A., Willman, B., Brooks, A. M., Governato, F., Brook, C. B., Hogg, D. W., Quinn, T., & Stinson, G. 2009, ApJ, 702, 1058

Table 1.   The number of stellar objects located in each annulus shown in Figure 1, and in each region shown in Figure 2. The sixth column includes all points out to a radius of $r \lesssim$ 3.75 degrees.

		Annuli (degrees)			
Region	0-1	1-2	2-3	3-3.75	All
M33 RGB	83394	7597	7235	3472	101698
MW Disk	9064	15431	26326	13716	64537
MW Halo	9894	4309	6784	3479	24466
Total within annulus	595878	163178	243949	148885	1151890

Table 2.   The fit parameters for the exponential model fits in Section 4.3 shown in Figure 7. Each column shows the quantity first in measured units, then in physical units in parentheses. Units for each column are shown as footnotes. The uncertainties on each parameter are shown under the columns labelled with Δ.

S/N	Σ_0 [a]	$\Delta\Sigma_0$ [a]	r_0 [b]	Δr_0 [b]	Σ_{bg} [c]	$\Delta\Sigma_{bg}$ [c]	χ^2
15	233 (3.7)	189 (3.0)	1.0 (14)	0.6 (8)	365 (5.7)	14 (0.2)	1.2
20	163 (2.6)	102 (1.6)	1.4 (20)	1.1 (16)	360 (5.6)	23 (0.4)	1.1
25	158 (2.5)	83 (1.3)	1.5 (21)	1.3 (18)	355 (5.6)	28 (0.4)	1.1
30	182 (2.9)	124 (1.9)	1.3 (18)	1.0 (14)	361 (5.7)	23 (0.4)	1.2

[a] Counts degree^{-2} (10^{-9} L$_\odot$ kpc^{-2}).

[b] Degrees (kpc).

[c] Counts degree^{-2} (10^{-9} L$_\odot$ kpc^{-2}).
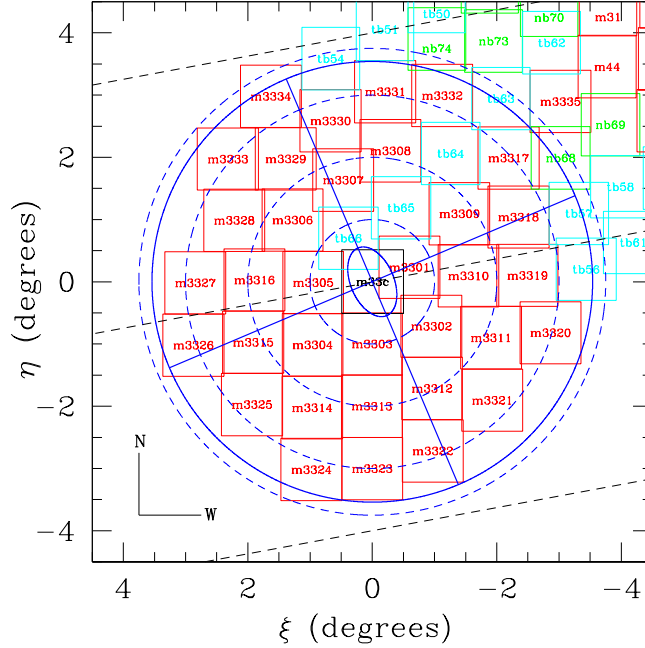
Fig. 1.— A tangent-plane projection of the PAndAS fields around M33. The central field, m33c (black), is from the archive (the data is from 2003B and 2004B). All other fields with prefix m (red) were observed in 2008B. Fields with prefix nb (green) and tb (light blue) were observed in 2009B and 2010B, respectively. The dark blue solid ellipse marks the diameter (73 x 45 arcminutes) at which $\mu_B \approx 25$ mag arcsec^{-2} (Nilson 1973). The two perpendicular lines show the major and minor axes (the major axis is inclined 23 degrees from the vertical; Nilson 1973). The solid-line circle represents $r = 50$ kpc ($\approx 0.33\ r_{M33,virial}$). The concentric dashed-line circles mark radii of $r = 1, 2, 3$ and 3.75 degrees (14.1, 28.2, 42.4 and 53.0 kpc, respectively). We assume a distance modulus of $(m - M_0) = 24.54 \pm 0.06$ (809±24 kpc; McConnachie et al. 2004, 2005). The three straight black dashed lines each represent one line of equivalent Galactic latitude (b = -35.3, -31.3 and -27.3).
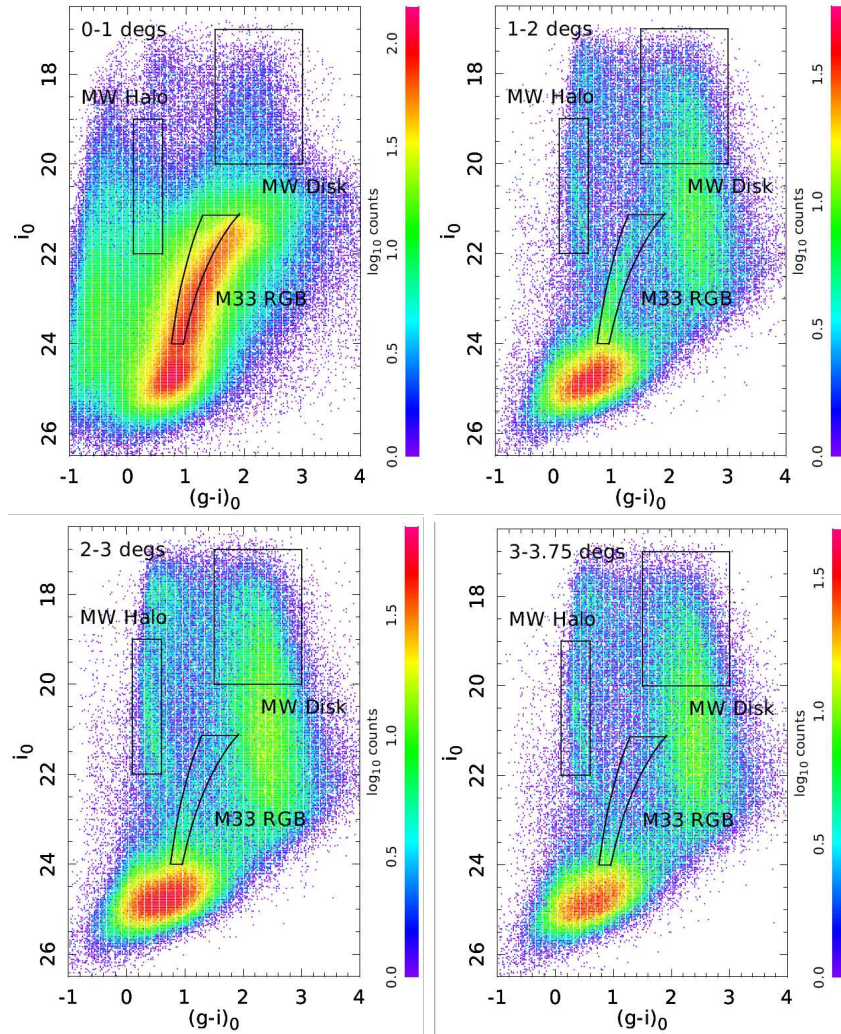
Fig. 2.— Color-magnitude (Hess) diagrams of the different annuli shown in Figure 1. Bins are 0.025 x 0.025 mag, and are shown with a logarithmic scaling in number counts of stars. Contamination due to the foreground MW **halo** and **disk** stars is estimated with the regions defined by $0.1 < (g - i)_0 < 0.6$, $19 < i_0 < 22$, and $1.5 < (g - i)_0 < 3$, $17 < i_0 < 20$, respectively (shown as the boxes in each panel). The isochrones correspond to [Fe/H] = -1.0 and -2.5 dex for a 12 Gyr, [α/H]=0.0 stellar population at the distance of M33, and have magnitude limits of $21.0 < i_0 < 24.0$. The annulus between $3 < r \leq 3.75$ degrees was used to determine the levels of foreground contamination. The bright clump at $i_0 \sim 25$, $0 < i_0 < 1$ is mainly composed of misclassified background galaxies (with a very small number of M33 horizontal-branch/red-clump stars).
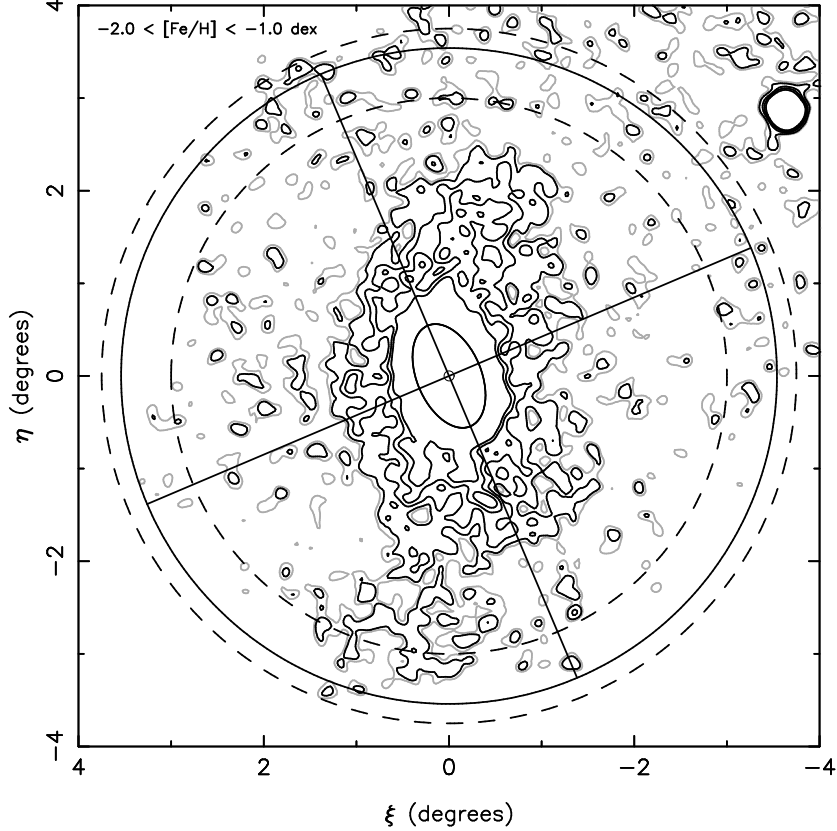
Fig. 3.— Density contours of candidate RGB stars similar to Figure 13 in McConnachie et al. (2010) but updated using data from 2010B for frames tb62-tb66 (see Figure 1). The grey contour is 1σ above the background, corresponding to an estimated surface brightness limit of $\mu_V = 33.0$ mag arcsec^{-2}. We exclude regions within this contour for our estimate of the stellar halo. The black contours correspond to 2, 5, 8 and 12σ above the background ($\mu_V \approx$ 32.5, 31.7, 31.2, and 30.6 mag arcsec^{-2}, respectively). The feature at $(\xi, \eta = (\text{-}3.5, 3.6)$ is Andromeda II.
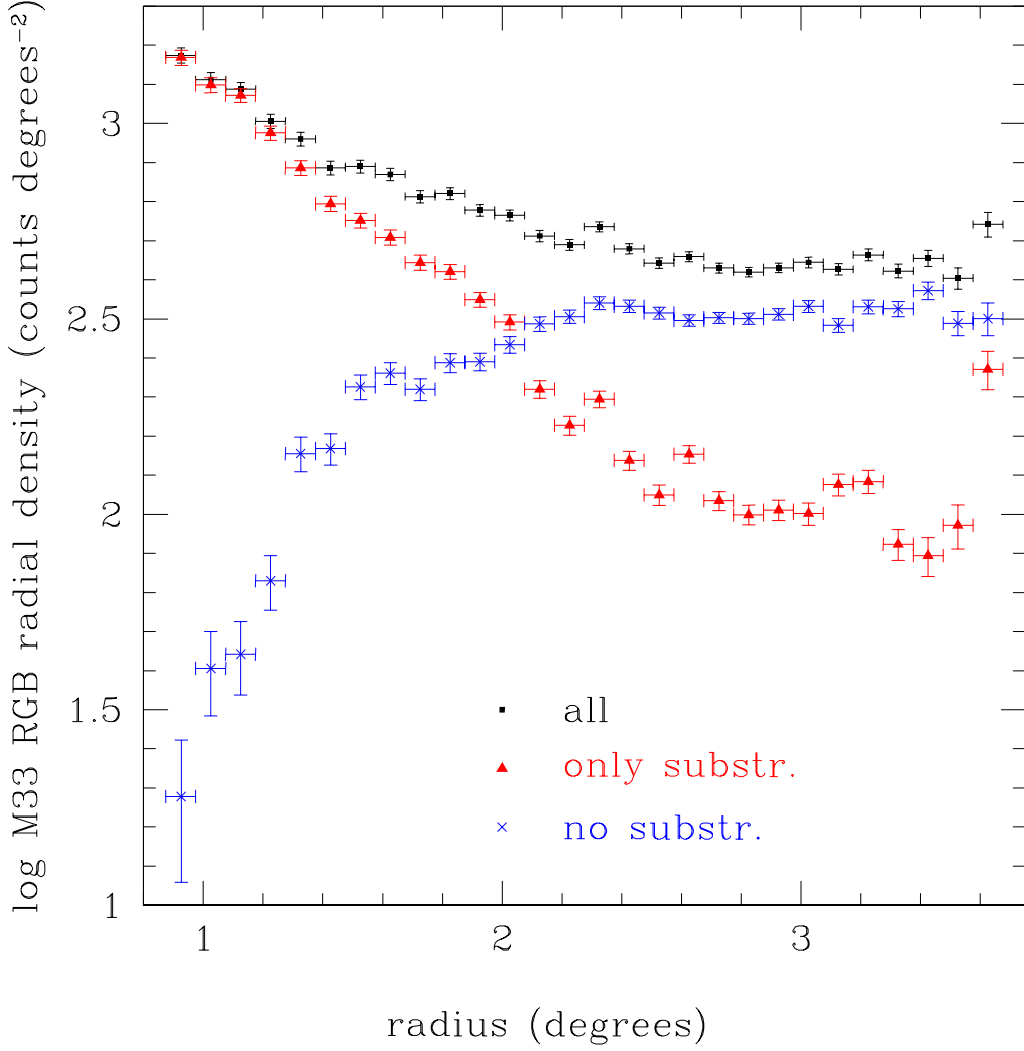
Fig. 4.— The radial profiles of extended disk substructure (red triangles) and non-substructure (blue crosses) regions, identified by the grey 1σ contours in Figure 3, normalized using the total annulus area. The total radial profile is shown by the black squares. We only show the profiles beginning at $\sim$0.85, within which the extended disk substructure completely dominates. Each bin location is fixed for all three components, and all bins have a fixed width of 0.1 degrees (shown by the horizontal error bars). The vertical error bars show $\sqrt{n}/$area.
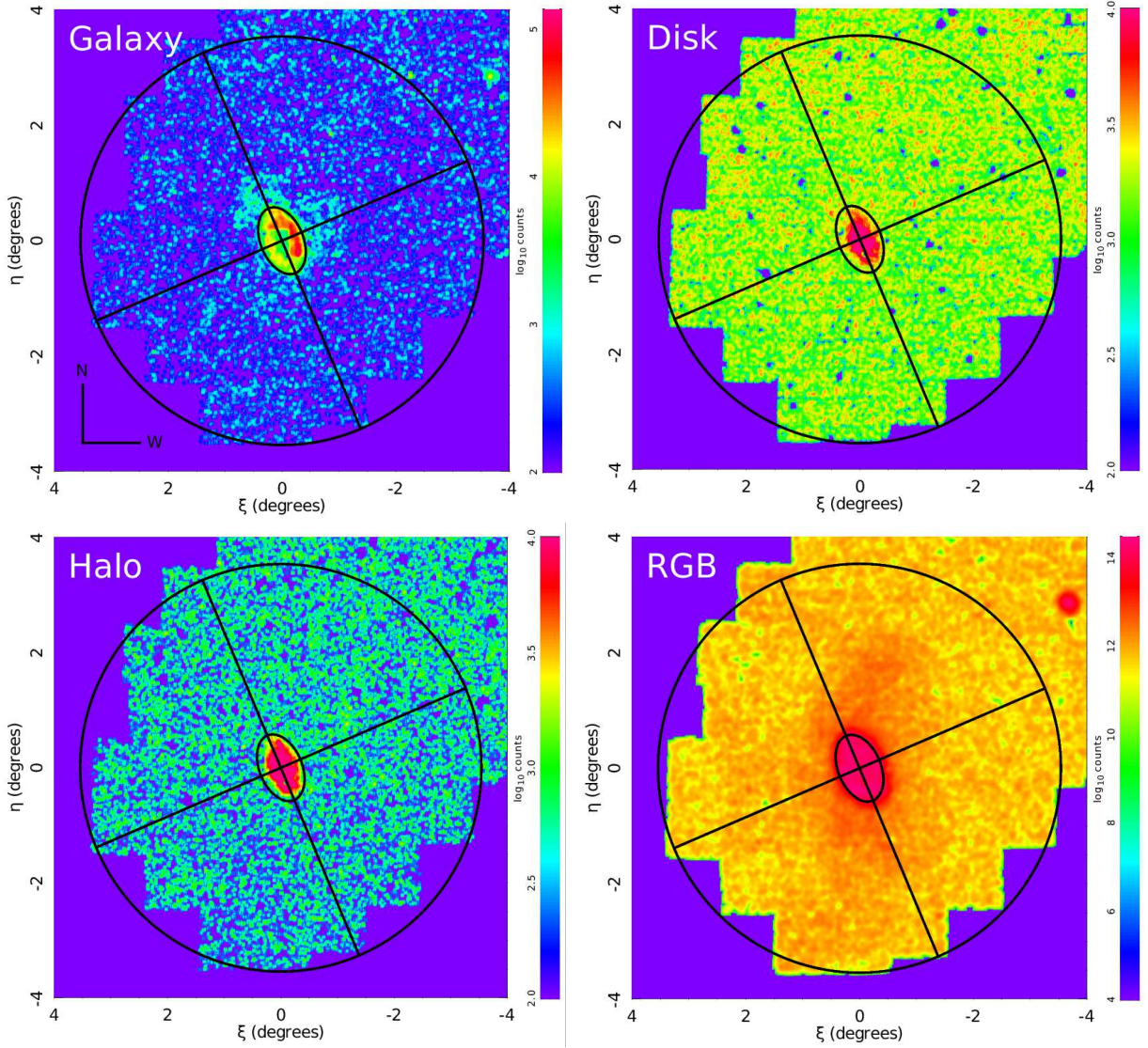
Fig. 5.— Smoothed maps of the spatial distribution maps for the candidate galaxies, MW disk, MW halo and M33 RGB stars. See Section 4 for details. Clearly visible in the RGB map (-2.5 < [Fe/H] < -1.0 dex) are the M33 extended disk substructure and Andromeda II in the NW. The ellipse, two perpendicular lines and circle are as in Figure 1. To ensure the most effective colour range to show features (or lack thereof), zeropoints were set at log counts = 2 for the galaxy, disk and halo plots, and log counts = 4 for the RGB plot.
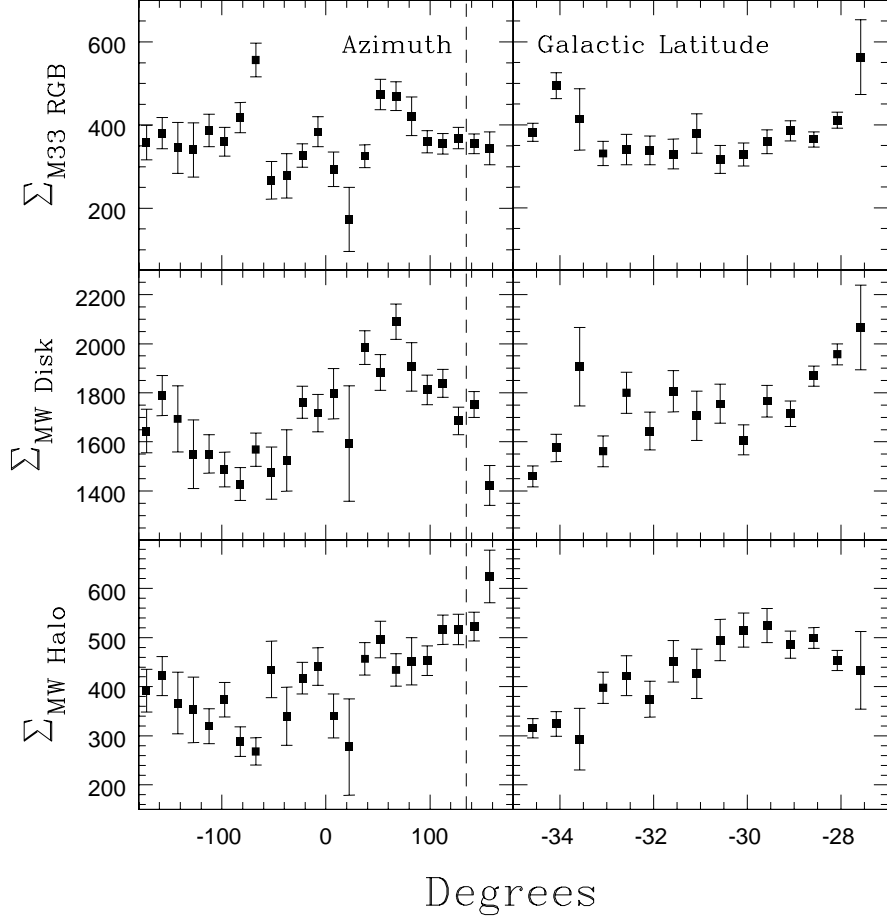
Fig. 6.— The left- and right-hand columns show the azimuthal and Galactic latitudinal distributions, respectively, of the density (counts degree^{-2}) variations for each region in Figure 2. The data within the $3 < r \leq 3.75$ degree annulus, having excised the area associated with the extended disk substructure, is shown. For the azimuthal distributions, 0, 90, ±180, and -90 degrees correspond to east, north, west and south, respectively. M31's centre is at approximately 135 degrees in this orientation (as indicated by the dashed line). The errors in all panels correspond to the values of $\sqrt{n}$/area.
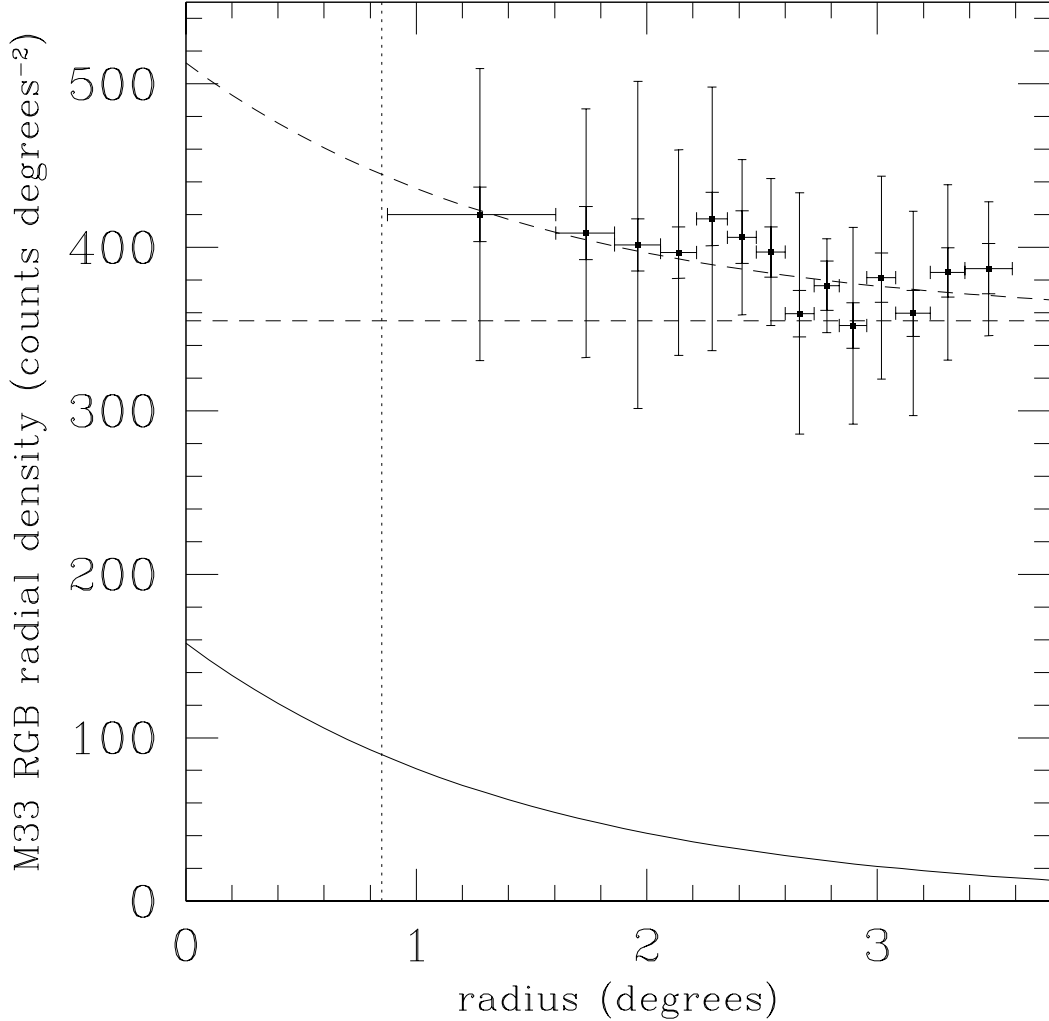
Fig. 7.— The background-uncorrected (upper dashed curved line and points) and the background-corrected (lower solid curved line) radial profiles of RGB candidate stars. The horizontal dashed line indicates the background level, Σ_{bg}. Two radial density (vertical) error bars are shown: the smaller set is calculated using $\sqrt{n}/$area as the error in each bin. The bin size was allowed to vary until the required signal-to-noise ratio of 25 was reached. Horizontal "error" bars show the width of the bin. The vertical dashed regions indicate the radius within which we do not have any data because we excise the area dominated by the disk and extended disk substructure surrounding the disk. The larger vertical error bars show the variation due to residual substructure (see Section 4.3 for details).
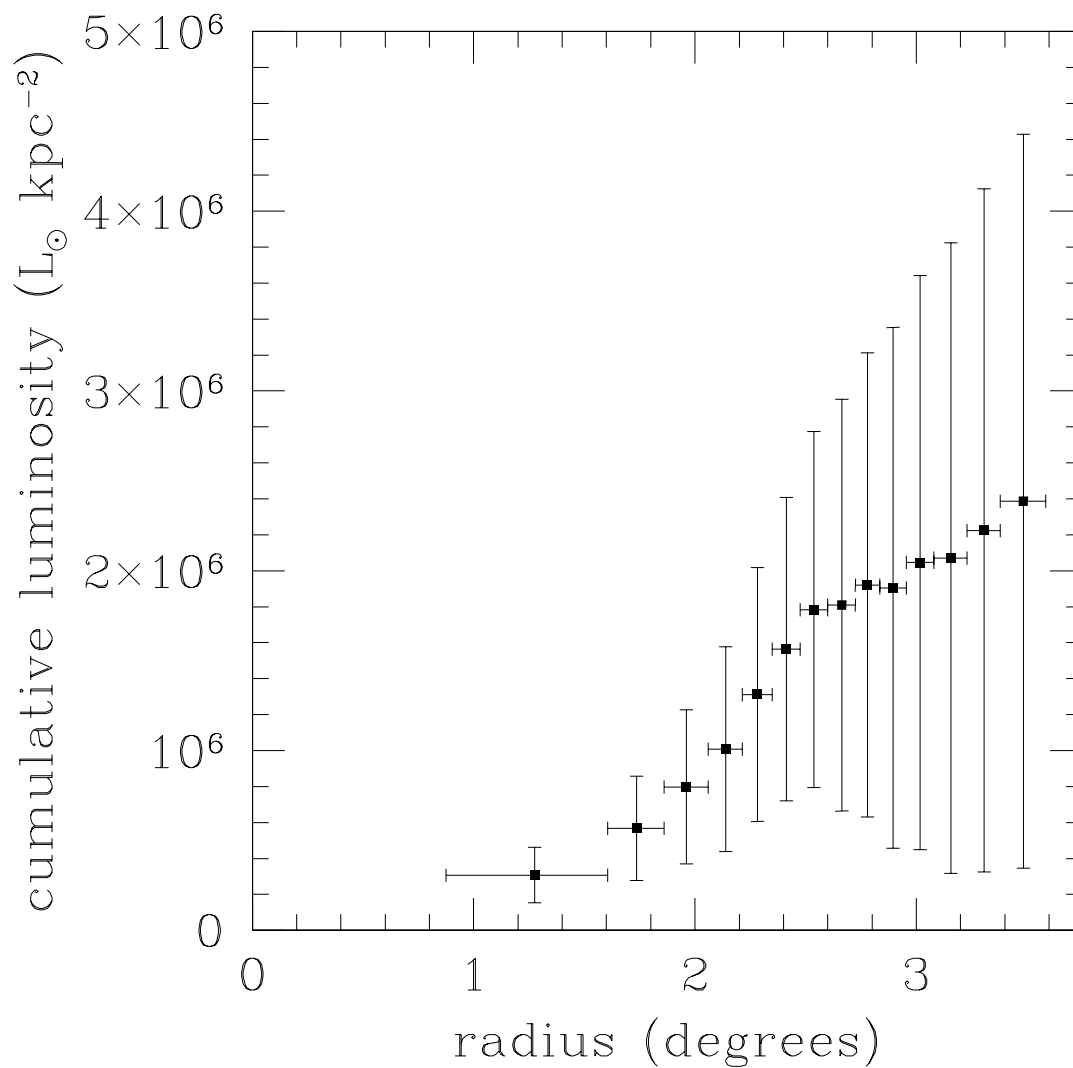
Fig. 8.— The cumulative luminosity as a function of radius. Horizontal "error" bars show the width of the bin, and are the same as those shown in Figure 7. The error on the luminosity is calculated by combining the Poisson errors for the RGB candidate star counts with the uncertainty of the background. This figure highlights the increase in our estimate of the luminosity uncertainty as we increase the area we consider.
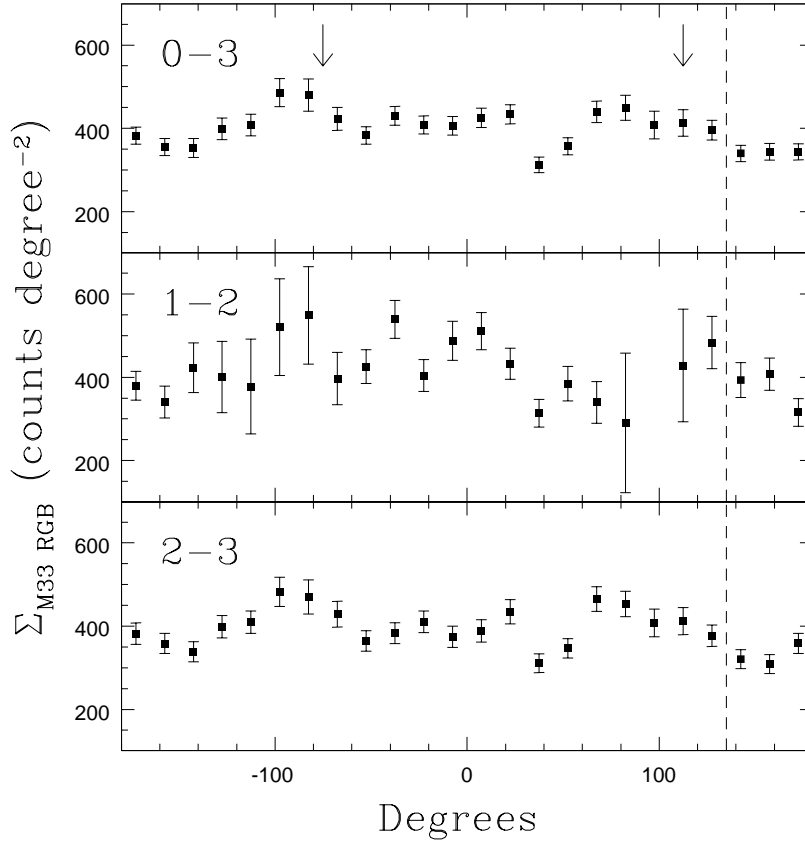
Fig. 9.— The azimuthal distribution of RGB candidate stars for the annuli shown in the top left of each plot. 0, 90, $\pm$180, and -90 degrees correspond to east, north, west and south, respectively. M31's centre is at approximately 135 degrees in this orientation (as indicated by the dashed line). The top, middle and bottom panels show the data with $r < 3$, $1 < r < 2$, and $2 < r < 3$ degrees, with the regions associated with the extended disk substructure excised in all panels. The left- and right-hand arrows correspond approximately to the SE and NW tips of the S-shaped warp of the extended disk substructure.
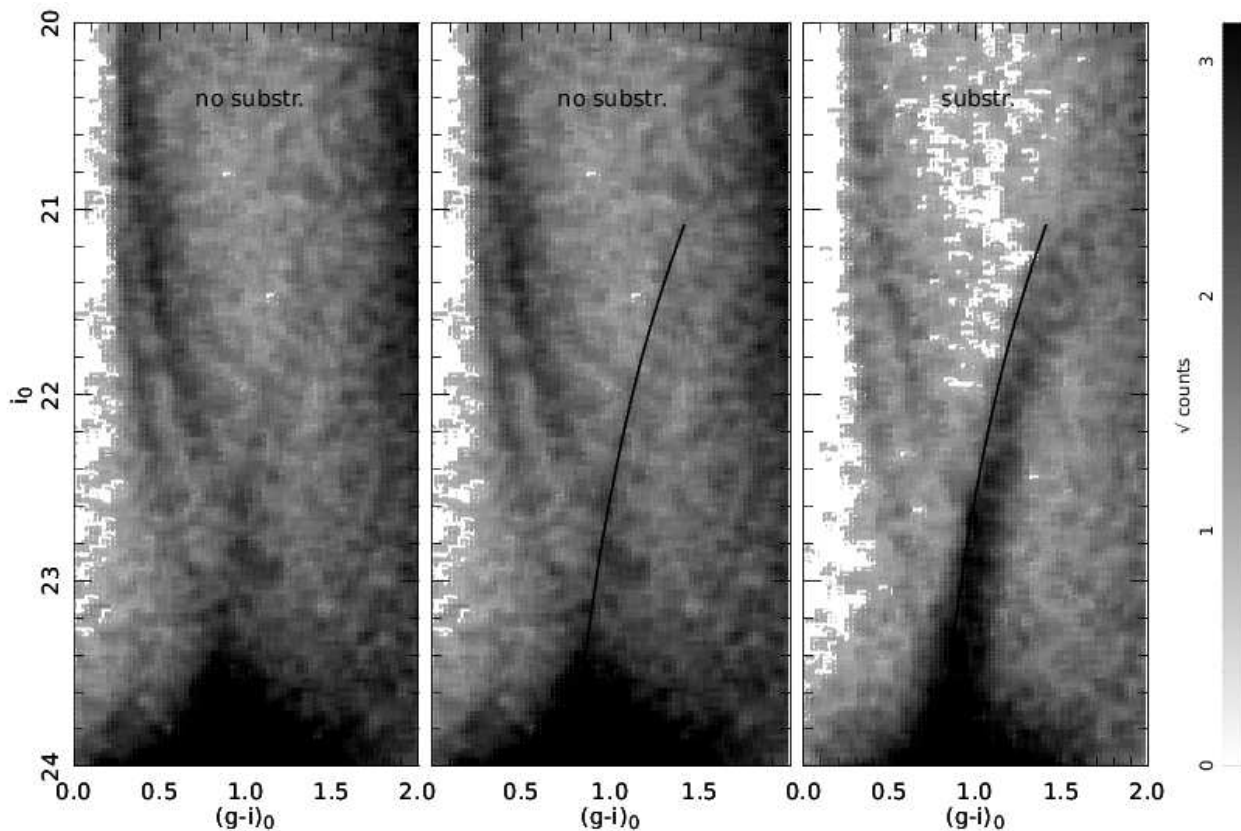
Fig. 10.— Similar to Figure 2, but here showing the CMD for the region with $r < 3$ degrees. The left-hand and middle panels show the CMD after excising the extended disk substructure areas in Figure 3 (which effectively imposes a minimum radius of $r = 0.88$ degrees). The RGB that we aim to detect is so faint that it is barely visible on the left hand plot. We overlay a $[Fe/H] = -2$ dex isochrone on the middle plot. The right-hand plot shows the CMD of the extended disk substructure areas for comparison.
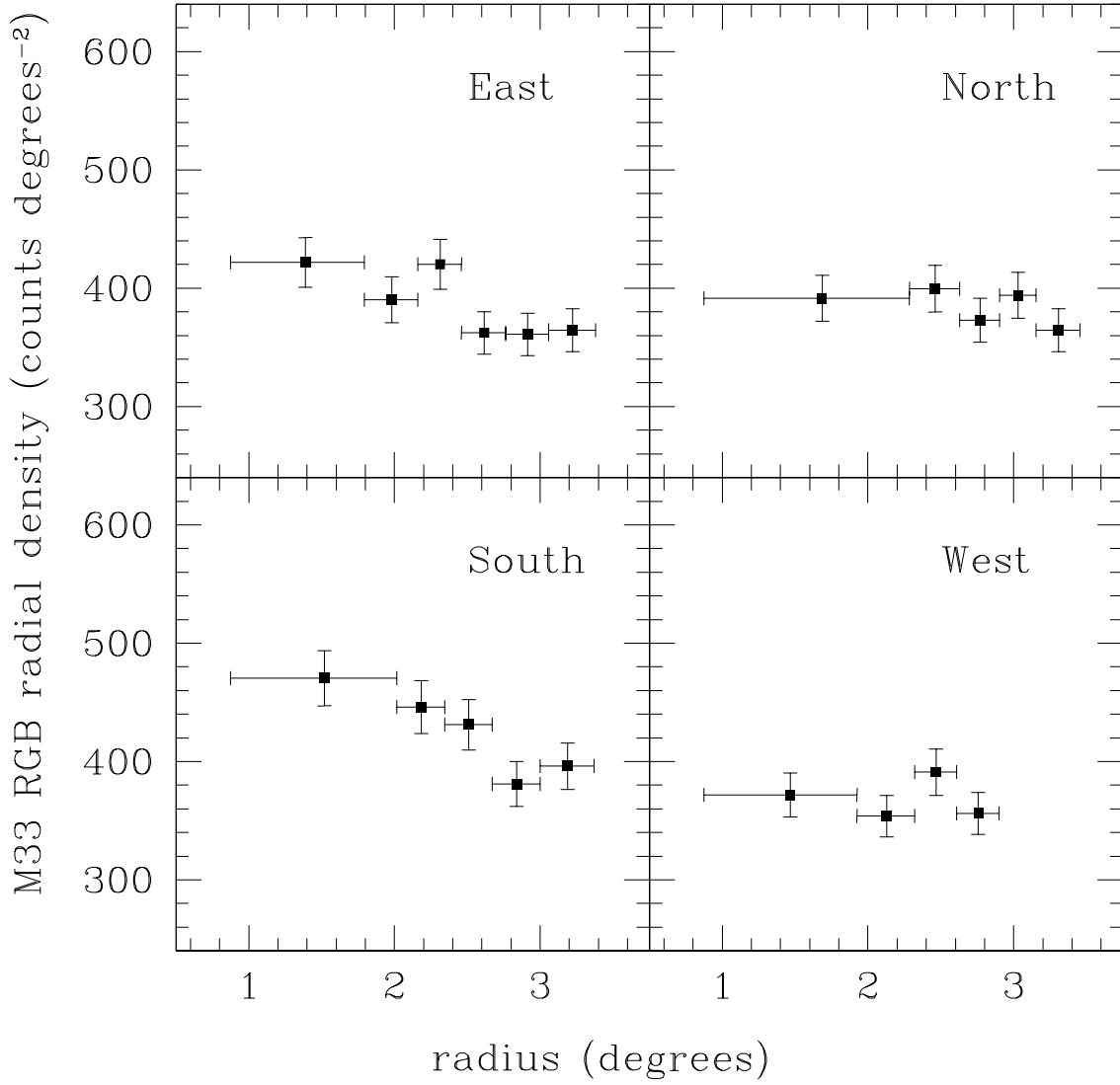
Fig. 11.— Background-uncorrected profiles for the quadrants split by major and minor axes, e.g., as shown in Figure 3.
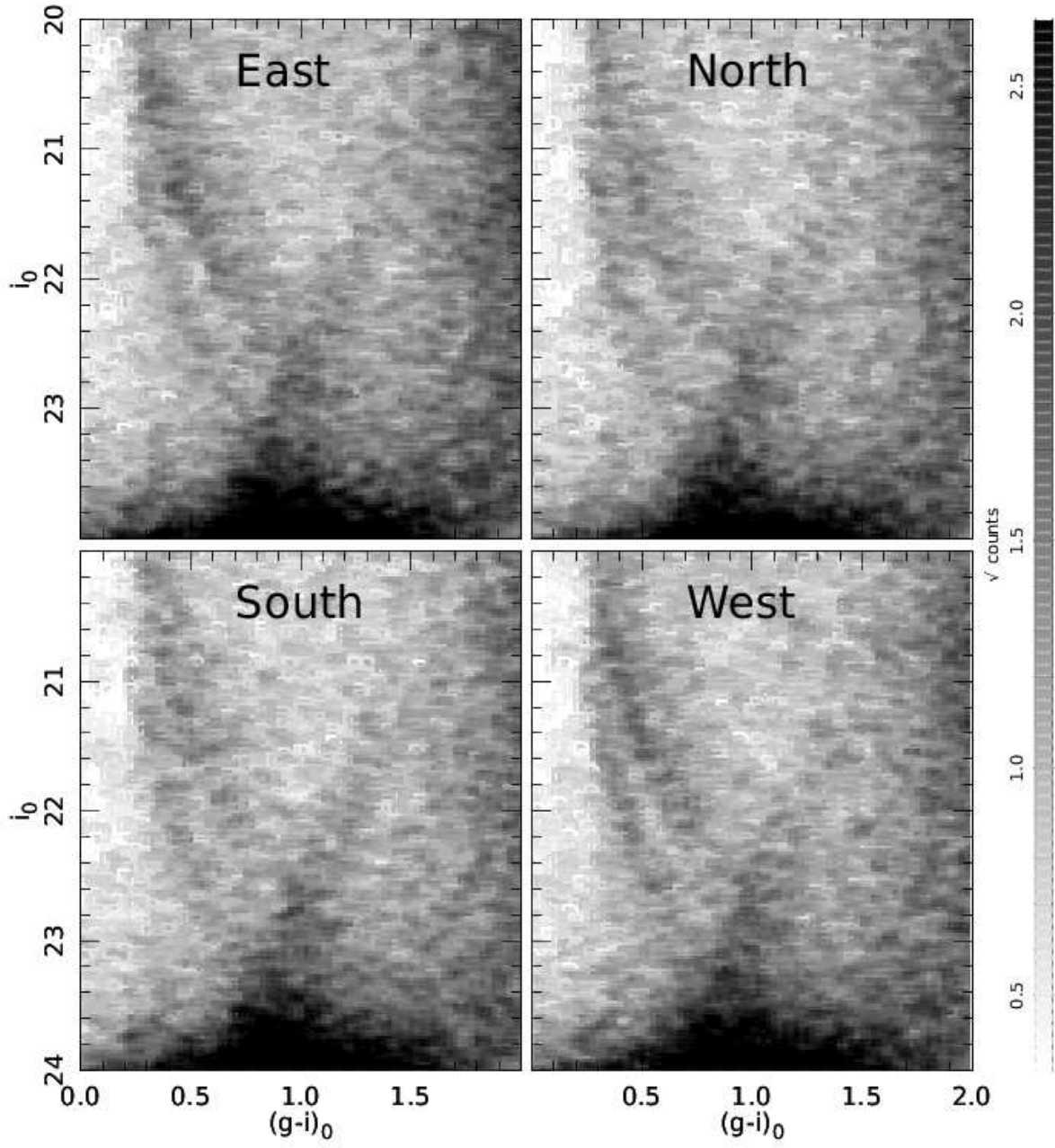
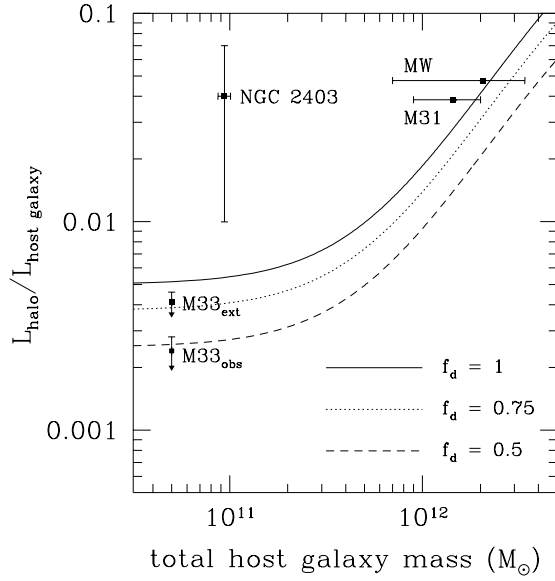Fig. 12.— The CMDs for the quadrants used in Figure 11.

Fig. 13.— The halo luminosity as a fraction of the host galaxy luminosity against the total host galaxy mass (dark plus luminous) for the MW, M31, M33 and NGC 2403. Data for the MW, M31 and NGC 2403 are from the literature (see Sections 2.1, 2.2 and 5, respectively, for details and references). M33's host galaxy mass is from Corbelli & Salucci (2000). The ranges of M33's halo luminosity are our estimates from this paper. The observed range comes from strictly limiting the integration between the range of our actual data, whereas the extrapolated range comes from extrapolating inwardly to the centre of M33 and outwardly to M33's virial radius. The lines represent the models for the intrahalo light fraction in Purcell et al. (2007). We use $n_{eff} = 1$ in conjunction with the three values for f_d shown in the plot. n_{eff} represents the effective number of satellites with mass $M_{sat} = M_{host}/20$; f_d represents the total stellar mass fraction a satellite contributes to its host galaxy halo. No distinction is made between halo substructure and a smooth halo component for the host luminosity estimates in the literature for the MW, M31, and NGC 2403 - similarly for the Purcell et al. models. McConnachie et al. (2010) estimate the luminosity of the extended disk substructure (EDS), $L_{EDS} \approx 0.01 L_{M33}$ so $L_{EDS} \approx 10^7 L_\odot$. M33's extended disk substructure is in the halo region, and if it was to be included in the estimates shown in this figure it would raise each $L_{halo}/L_{hostgalaxy}$ estimate by 0.01.